1 **Second-generation stoichiometric mathematical model to predict methane**
2 **emissions from oil sands tailings**

3 Jude D. Kong[1,2], Hao Wang[2*†], Tariq Siddique[3*‡], Julia Foght[4], Kathleen Semple[4], Zvonko

4 Burkus[5], and Mark A. Lewis[2,4]

5 [1]Center for Discrete Mathematics and Theoretical computer Science, Rutgers University, 96

6 Frelinghuysen Road Piscataway, NJ 08854-8018, USA

7 [2]Department of Mathematical and Statistical Sciences, University of Alberta, Edmonton, AB

8 T6G 2G1, Canada

9 [3]Department of Renewable Resources, University of Alberta, Edmonton, AB T6G 2G7, Canada

10 [4]Department of Biological Sciences, University of Alberta, Edmonton, AB T6G 2E9, Canada

11 [5]Alberta Environment and Parks, Government of Alberta, Edmonton, Canada

12

13 Corresponding authors' emails:

14 [*†] Mathematical approach (Hao Wang); hao8@ualberta.ca

15 [*‡] Biological approach (Tariq Siddique); tariq.siddique@ualberta.ca

16 **Abstract**

17

18 Microbial metabolism of fugitive hydrocarbons produces greenhouse gas (GHG) emissions from

19 oil sands tailings ponds (OSTP) and end pit lakes (EPL) that retain fluid tailings from surface

20 mining of oil sands ores. Predicting GHG production, particularly methane (CH_4), would help oil

21 sands operators mitigate tailings emissions and may assist regulators evaluating the trajectory of

22 reclamation scenarios. Using empirical datasets from laboratory incubation of OSTP sediments

23 with pertinent hydrocarbons, we developed a stoichiometric model for CH_4 generation by

24   indigenous microbes. This model improved on previous first-approximation models by

25   considering long-term biodegradation kinetics for 18 relevant hydrocarbons from three different

26   oil sands operations, lag times, nutrient limitations, and microbial growth and death rates.

27   Laboratory measurements were used to estimate model parameter values and to validate the new

28   model. Goodness of fit analysis showed that the stoichiometric model predicted CH_4 production

29   well; normalized mean square error analysis revealed that it surpassed previous models.

30   Comparison of model predictions with field measurements of CH_4 emissions further validated

31   the new model. Importantly, the model also identified parameters that are currently lacking but

32   are needed to enable future robust modeling of CH_4 production from OSTP and EPL in-situ.

33

34   **Keywords:** modeling methane production; anaerobic hydrocarbon biodegradation;

35   methanogenesis; greenhouse gas emissions; oil sands tailings pond; end pit lake

1. Introduction

Alberta's oil sands industry is a major economic driver in Canada, currently producing ~3 million barrels oil d^{-1} and expected to reach 4 million barrels d^{-1} by 2024 (Government of Alberta, 2019a; https://aer.ca/providing-information/data-and-reports/statistical-reports/st53). However, the oil sands sector has come under international scrutiny regarding GHG emissions and other environmental issues. Oil sands operations including mining, upgrading and in-situ extraction were responsible for ~43% of Alberta's overall GHG emissions in 2012 (Alberta Greenhouse Gas Report, 2016). In addition to these production operations, the storage and management of aqueous slurries of surface-mined ore processing wastes in oil sands tailings ponds (OSTP; Figure S1) contributes substantially to methane (CH_4) and carbon dioxide (CO_2) emissions (Burkus et al., 2014; Siddique et al., 2008). Total fugitive GHG emissions from major oil sands operators' OSTP, measured in-situ using floating flux chambers in 2011, were calculated to be 2.8 million tonnes CO_2 equivalent per year (Burkus et al., 2014), while in 2018 they were estimated at ~2.2 Mt of CO_2e (Z. Burkus, personal communication). Furthermore, proposed implementation of EPL as a long-term reclamation strategy for OSTP sediments (Figure S1) may contribute additional GHG emissions for an unknown timespan.

During five decades of retention, enormous volumes of tailings have accumulated that is currently estimated at >1.2 billion m^3 (Government of Alberta, 2019b). As the fluid tailings in OSTP age, the suspended clay fines settle via several mechanisms (porewater and solid phase chemistry) including gravity (Siddique et al., 2014) to become anaerobic mature fine tailings (MFT) having a solids content >30 wt% and possessing both an active microbiota and residual diluent in progressive stages of selective biodegradation (Fig S2 in Foght et al., 2017). The use of EPL has been discussed to reintegrate the accumulated tailings into the on-site environment (Charette et al., 2012) and proposed by industry in their tailings management plans as one of their closure approaches (Alberta Energy Regulator, 2019). In this reclamation scenario, after

60 years or decades of residence in OSTP, MFT would be treated and transported to mined-out pits

61 and capped with fresh water and/or process-affected water. This is intended to establish a

62 sustainable aquatic system (i.e., an end pit lake; EPL) that, with time, should support economic,

63 ecological and/or societal uses (Charette et al., 2012). However, ebullition of GHG from

64 underlying sediments may delay EPL ecosystem development by dispersing fine sediments into

65 the overlying water layer along, potentially co-transporting some constituents of concern. Thus,

66 GHG emissions from oil sands tailings repositories are problematic from global warming as well

67 as ecological standpoints.

68   GHG emissions from OSTP and EPL result primarily from anaerobic biodegradation of

69 diluent hydrocarbons, naphtha or light paraffins, introduced into tailings after aqueous extraction

70 of bitumen from oil sands ore and treatment of froth (Figure S1; reviewed in Foght et al., 2017)

71 The diluents, specific to each operator, facilitate separation of bitumen from water and mineral

72 solid particles during froth treatment and reduce bitumen viscosity in preparation for processing

73 and/or transport. Most of the diluent is recovered from the froth treatment tailings for re-use, but

74 a small proportion remains in the tailings slurry that comprises alkaline water, sand, silt, clays

75 and unrecovered bitumen. These fresh tailings, as well as other tailings streams that have not

76 been exposed to diluent, are deposited in OSTP where indigenous anaerobic microbial

77 communities biodegrade the labile hydrocarbons to CH_4 and CO_2 (Abu Laban et al., 2015;

78 Penner and Foght, 2010; Mohamad Shahimin et al., 2016; Siddique et al., 2011). Although

79 naphtha and paraffinic diluents are considered to be the major carbon sources for microbes in

80 OSTP (Foght et al., 2017), only certain of their hydrocarbon components are known to be

81 biodegradable under anaerobic conditions, whereas others are recalcitrant (slowly or

82 incompletely biodegraded) or are completely resistant to biodegradation (Siddique et al., 2018).

4

83 Although bitumen is the overwhelming organic constituent of fresh tailings, it predominantly

84 comprises recalcitrant hydrocarbons: only a small proportion may be labile and the contribution

85 of bitumen to biogenic GHG is thought to be negligible in proportion to that of diluent (Foght et

86 al., 2017).

87 The importance of modeling GHG emissions is clear to oil sands operators, as it provides a

88 rationale for mitigating GHG mitigation efforts and managing OSTP and EPL. However, field

89 data (e.g., concentrations of individual hydrocarbons in OSTP, nutrient concentrations, biomass)

90 needed for modeling are generally unavailable either because collection of such data is

91 technologically difficult or because such key model parameters have not previously been

92 identified as necessary. Therefore, we have cultivated MFT in laboratory cultures analogous to

93 OSTP and EPL for use in initial modeling efforts. A previous study (Siddique et al., 2008) used

94 limited data available from short-term (<1 yr) laboratory studies measuring biodegradation of a

95 small subset of components (Siddique et al., 2007, 2006) in a single naphtha diluent to develop

96 zero- and first-order kinetic models for estimating CH_4 production potential from a single OSTP.

97 That first approximation model predicted in-situ CH_4 production volumes reasonably consistent

98 with emissions measured in-situ (Siddique et al., 2008). However, in the decade since that work,

99 additional components of naphtha and paraffinic diluent have been shown to support

100 methanogenesis from MFT during extended laboratory incubation (up to 6.5 y; Abu Laban et al.,

101 2015; Mohamad Shahimin et al., 2016; Siddique et al., 2015, 2011). This finding increases

102 theoretical GHG emissions, especially from hydrocarbons previously assumed to be recalcitrant

103 and thus not considered in the previous model and over extended time scales more relevant to

104 long-term retention of tailings. Additionally, data are now available for additional OSTP

105 receiving different diluents and therefore having unique microbial communities (Wilson et al.,

106 2016) with different CH_4 production potentials, and the effect of potentially growth-limiting

107 nutrients in-situ such as nitrogen has begun to be examined (Collins et al., 2016). Also, the first

108 EPL field trial was established in 2012/2013 where CH_4 has been detected within the water cap

109 (Risacher et al., 2018). The greatly expanded data set and a broader understanding of oil sands

110 tailings microbiology (Foght et al., 2017) enable and have driven development of the improved

111 and flexible model for CH_4 generation described here.

112   The goals of the new stoichiometric model were: (1) to expand CH_4 predictive capability by

113 considering methanogenic biodegradation of a wider range of hydrocarbons only recently shown

114 to be labile over longer incubation times; (2) for the first time to consider OSTP that receive

115 diluents having different compositions and that harbour different microbial communities; (3) to

116 account for the effects of nutrient limitation on CH_4 generation, particularly available nitrogen;

117 (4) to compare model predictions with field measurements of CH_4 emissions to validate the

118 model and reveal any shortcomings; (5) to consider differences in GHG emission trajectories

119 between OSTP and EPL; and (6) to identify parameters essential for future development of a

120 model to predict CH_4 emissions in-situ in OSTP and EPL.

121 **2. Materials and Methods**

122 Although the gaseous products of methanogenic hydrocarbon biodegradation are CH_4 and CO_2

123 (Figure S2), the stoichiometric model developed here considers only CH_4 production for two

124 reasons: CH_4 has a greater greenhouse effect than CO_2; and measurement of emissions of CO_2

125 emissions produced in MFT is confounded by abiotic (carbonate dissolution) and

126 biogeochemical (mineral precipitation and dissolution) interactions with tailings minerals

127 (Siddique et al., 2014), complicating measurement and modeling.

128   Methane production from hydrocarbons involves two microbial processes: the oxidation of

129   labile hydrocarbons to simple organic compounds by Bacteria and the conversion of those

130   compounds to CH_4 and CO_2 by Archaea (Figure S2). Therefore, the model was developed in two

131   modules. The first module (section 2.1) comprising two systems of equations describes bacterial

132   biodegradation of 18 hydrocarbon substrates (see section 2.3.1 for selection rationale) and

133   includes formation of microbial biomass. The second module (section 2.2) considers archaeal

134   CH_4 generation from bacterial metabolites. Model parameters unavailable in the literature were

135   estimated by data fitting using laboratory measurements (section 2.3). The model then was

136   quantitatively validated by comparison (1) to measurements from independent but analogous

137   laboratory experiments conducted using oil sands tailings incubated with whole diluents or

138   components of naphtha or paraffinic diluents and (2) to field measurements of CH_4 emissions

139   from OSTP (section 2.4). Finally the model was qualitatively assessed using phase plane analysis

140   to illustrate CH_4 emission trajectories in OSTP and EPL (section 2.5 and supporting material

141   section S3). Terms used in model development are defined in Table 1.

142   *2.1 Biodegradation and biomass module development.*

143   Direct measurement of hydrocarbon biodegradation kinetics in OSTP and EPL is technically

144   infeasible. Therefore this module describes the dynamics of CH_4 production from MFT

145   incubated with cognate naphtha or paraffinic diluents under laboratory conditions analogous to

146   those expected in OSTP or EPL. A brief description of previously published cultivation methods

147   used to generate model data is given in supporting material section S1.

148   Microbial biomass can change as a result of growth and death. Because hydrocarbon

149   biodegradation is initiated by Bacteria and not by the archaeal methanogens (Figure S2), this

150   module considers only bacterial kinetics. The per cell bacterial growth rate is assumed to follow

7

151 Liebig's law of the minimum (Sterner and Elser, 2002) stating that growth rate is proportional to

152 the most limiting resource available. The model assumes, based on chemical analysis of oil sands

153 tailings (Collins, 2013; Penner and Foght, 2010) that all relevant nutrients except biologically-

154 available nitrogen (defined in Table 1) and/or labile carbon are present at non-limiting

155 concentrations in OSTP and EPL. Therefore the bacterial growth rate is modeled as a function

156 only of the mass of biologically-available nitrogen (N_A) and labile hydrocarbons (C_i, the mass of

157 labile hydrocarbons in the system for $i=1...n$, assuming n discrete labile hydrocarbons in the

158 system). Assuming that there is negligible input of N_A with fresh tailings, no outflow of soluble

159 N_A and no loss of gaseous NO_x, we take the total nitrogen (N_T) in these systems to be constant.

160 With this assumption, the subset of N_T available for bacterial growth (N_A) is given by $N_A = N_T-$

161 θB where θ is the ratio of nitrogen to carbon in the total microbial biomass B, and θ is assumed

162 to be constant (Makino et al., 2003). The Monod functions $f(N_A) = \frac{N_A}{N_A+K_f}$ and $g(C_i) = \frac{C_i}{C_i+K_{g_i}}$

163 are used to model the nitrogen- and carbon-dependent growth rates respectively, where K_f is the

164 N_A-dependent half-saturation constant; K_{g_i} is the C_i-dependent half-saturation constant; and C_i^{in}

165 is the inflow of C_i to the system. Thus, the C_i-dependent per cell bacterial growth rate μ is given

166 by $\mu_i \min\{f(N_A), g(C_i)\}$, where μ_i is the maximum growth rate of bacteria growing on only the

167 hydrocarbon C_i present and is unique for each labile hydrocarbon. Hence the total per cell

168 growth rate of bacteria is $\sum_{i=1}^{n} \mu_i \min\{f(N_A), g(C_i)\}$.

169 The biodegradation rate of each labile hydrocarbon i is assumed to be proportional to the

170 bacterial growth rate due to its consumption, i.e., [per cell bacterial growth rate due to each

171 hydrocarbon] $\propto$ [biodegradation rate of hydrocarbon]. This implies that [the per cell bacterial

172 growth rate supported by each labile hydrocarbon i)] $= r_i$[the per cell biodegradation rate of that

173 hydrocarbon] where r_i is a proportionality constant reflecting the efficiency of bacterial

8

174   conversion of substrate into biomass. Hence, [the per cell biodegradation rate of each labile

175   hydrocarbon] $= \frac{1}{r_i}$ [the per cell bacterial growth rate supported by labile hydrocarbons], i.e., [the

176   per cell biodegradation rate of each hydrocarbon] $= \sum_{i=1}^{n} \frac{1}{r_i} \mu_i \min\{f(N_A), g(C_i)\}$. Archaeal

177   growth and death are considered in the second module (section 2.2).

178   We assume that microbial death rate (d) is constant in the laboratory cultures and that

179   nutrients in dead microbial biomass are quickly recycled back into labile carbon and nitrogen

180   (N_A). The fraction of C_i recycled from dead biomass b is assumed to be a constant β_i where $0 <$

181    $\beta_i < 1$.

182   In accordance with laboratory observations (Mohamad Shahimin and Siddique, 2017a,

183   2017b, Siddique et al., 2007, 2006), the model assumes that onset of biodegradation of each

184   hydrocarbon begins after a unique lag period, λ_i. The above assumptions lead to the following

185   system of equations:

186    $g(C_i) = \begin{cases} 0, & t < \lambda_i \\ \dfrac{C_i}{K_{g_i} + C_i}, & t \geq \lambda_i \end{cases}$

187    $\dfrac{dB}{dt} = B \sum_{i=1}^{n} \mu_i min\left\{\dfrac{N_A}{K_f + N_A}, g(C_i)\right\} - dB,$ (1)

188    $\dfrac{dC_i}{dt} = \dfrac{-1}{r_i} \mu_i B min\left\{\dfrac{N_A}{K_f + N_A}, g(C_i)\right\} + \beta_i dB + C_i^{in},$

189    $N_A = N_T - \theta B,$

190    $B(0) > 0, C_i(0) \geq 0.$

191   Since the carbon- and nutrient-dependent growth efficiency parameters describe the main

192   differences in bacterial utilization of different hydrocarbon, the model assumes that parameters

193   such as carbon conversion efficiency, intrinsic bacterial growth rate, and carbon recycling from

194   dead bacteria (negligible in our data fitting), are equivalent for different hydrocarbons; i.e., $\mu_i =$

195     $\mu, r_i = r$, and $\beta_i = \beta$. With this assumption, the system of equations becomes:

196

197     $$g(C_i) = \begin{cases} 0, & t < \lambda_i \\ \dfrac{C_i}{K_{g_i} + C_i}, & t \geq \lambda_i \end{cases}$$

198     $$\frac{dB}{dt} = B \sum_{i=1}^{n} \mu min \left\{ \frac{N_A}{K_f + N_A}, g(C_i) \right\} - dB, \qquad\qquad (2)$$

199     $$\frac{dC_i}{dt} = \frac{-1}{r} \mu B min \left\{ \frac{N_A}{K_f + N_A}, g(C_i) \right\} + \beta dB + C_i^{in},$$

200     $$N_A = N_T - \theta B,$$

201     $$B(0) > 0, C_i(0) \geq 0.$$

202   To analyze the types of solutions that this model could produce, a steady state analysis was

203   performed. The algebraic analysis is described in supplementary material section S2 and is of

204   particular use because it allows solutions to be classified by parameter values.

205   *2.2 Methane biogenesis module development*

206   From the preceding biodegradation module, bacterial biodegradation of a hydrocarbon substrate

207   (C_i) per unit time yields $\frac{1}{r} \mu B min \left\{ \frac{N_A}{K_f + N_A}, g(C_i) \right\}$ units of metabolite(s) corresponding to C_i. The

208   metabolite(s) ultimately are converted to CH_4 and CO_2 (G_i) by methanogens (Figure S2). Since

209   methanogens have a slow growth rate compared to that of the hydrocarbon-degrading Bacteria

210   (being dependent on their metabolism), we assume that the biomass of methanogens in the

211   system is constant. With these additions, the system of equations (2) becomes:

212 $\quad (C_i) = \begin{cases} 0, & t < \lambda_i \\ \dfrac{C_i}{K_{g_i} + C_i}, & t \geq \lambda_i \end{cases}$

213 $\quad \dfrac{dB}{dt} = B \sum\limits_{i=1}^{n} \mu \min\left\{\dfrac{N_A}{K_f + N_A}, g(C_i)\right\} - dB,$ $\qquad\qquad$ (3)

214 $\quad \dfrac{dC_i}{dt} = \dfrac{-1}{r} \mu B \min\left\{\dfrac{N_A}{K_f + N_A}, g(C_i)\right\} + \beta dB + C_i^{in},$
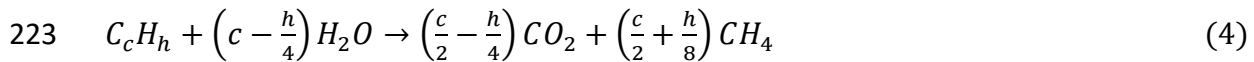
215 $\quad \dfrac{dG_i}{dt} = \dfrac{1}{r} \mu B \min\left\{\dfrac{N_A}{K_f + N_A}, g(C_i)\right\},$

216 $\quad CH_4 = \sum\limits_{i=1}^{n} \eta_i \Gamma_i G_i,$

217 $\quad N_A = N_T - \theta B,$

218 $\quad B(0) > 0, C_i \geq 0, G_i(0) = 0$

219 where, Γ_i is the maximum theoretical yield of CH4 expected from biodegradation of one mole of

220 C_i. This value can be calculated from Equation (4) (derived from Symons and Buswell, 1933, as

221 implemented by Roberts, 2002) that describes the complete oxidation of hydrocarbons to CH4

222 and CO2 under methanogenic conditions, namely:

223 $\quad C_cH_h + \left(c - \dfrac{h}{4}\right)H_2O \rightarrow \left(\dfrac{c}{2} - \dfrac{h}{4}\right)CO_2 + \left(\dfrac{c}{2} + \dfrac{h}{8}\right)CH_4$ $\qquad\qquad$ (4)

224 where c and h are, respectively, the numbers of carbon and hydrogen atoms in a C_i molecule.

225 $\qquad$ From equation (4), $\Gamma_i = \left(\dfrac{c}{2} + \dfrac{h}{8}\right)$. Furthermore, η_i is the fraction of the theoretical CH4 yield

226 from the biodegradation of a mole of C_i (i.e., a conversion efficiency factor) and is assumed to be

227 the same for all C_i, i.e., $\eta_i = \eta$, with $0 < \eta_i < 1$. The values of η_i used in numerical simulations

228 were obtained from (Mohamad Shahimin et al., 2016; Mohamad Shahimin and Siddique,

229 2017a, 2017b, Siddique et al., 2007, 2006) and Table S1.

230

2.3 Acquisition of laboratory data, parameter estimation and model validation

Our approach was to select a suite of 18 relevant labile hydrocarbons to generate model

predictions, then estimate missing model parameters using empirical biodegradation kinetics and

CH_4 measurements for these hydrocarbons, and finally to test the stoichiometric model

quantitatively using measurements from an independent set of laboratory experiments.

2.3.1 Model hydrocarbon selection and testing

Fugitive diluent in froth treatment tailings (Fig. S1) is the predominant substrate for

methanogenesis in OSTP (Foght et al., 2017). The most commonly used diluents are naphtha and

paraffinic solvent. Syncrude Canada Ltd. (Syncrude), Suncor, and Canadian Natural Resources

Ltd. (CNRL) use naphtha, the composition of which differs slightly for each company but which

comprises primarily paraffinic (*n-*, *iso-* and *cyclo-*alkanes) and monoaromatic hydrocarbons

(predominantly toluene and three xylene isomers), typically in the C_6-C_{10} range (Siddique et al.,

2008). Canadian Natural Upgrading Limited (CNUL; formerly Shell Albian), Imperial (Kearl

Mine) and Suncor (Fort Hills Mine) uses a paraffinic diluent comprising *n-* and *iso-*alkanes

primarily in the C_5-C_6 range (Mohamad Shahimin and Siddique, 2017a). Published results from

laboratory experiments incubating these whole diluents or their major constituents with MFT

from Syncrude, CNUL or CNRL (Mohamad Shahimin et al., 2016; Mohamad Shahimin and

Siddique, 2017a, 2017b, Siddique et al., 2007, 2006; and Table S1) revealed complete or

significant biodegradation of 18 hydrocarbons under methanogenic conditions, including the *n-*

alkanes *n*-pentane (C_5), *n*-hexane (C_6), *n*-heptane (C_7), *n*-octane (C_8), *n*-nonane (C_9), and *n-*

decane (C_{10}); the *iso-*alkanes 2-methylpentane (2-MC_5), 2-methylhexane (2-MC_6), 3-

methylhexane (3-MC_6), 2-methylheptane (2-MC_7), 4-methylheptane (4-MC_7), 2-methyloctane

253   (2-MC$_8$), 3-methyloctane (3-MC$_8$) and 2-methylnonane (2-MC$_9$); and the monoaromatics

254   toluene, *o*-xylene and *m*- plus *p*-xylenes (the latter two are not resolved by our gas

255   chromatography column and are therefore reported as a sum). Table 2 lists the 18 labile

256   hydrocarbons selected for model development, the source of biodegradation data, the type of

257   tailings used to generate the data and the parameters estimated using those data.

258   *2.3.2 Parameter estimation*

259   The values of many model parameters in the system of equations (3) are not available in the

260   literature, including the initial microbial biomass in OSTP and EPL (B(0)), the nitrogen half-

261   saturation constant (K$_f$), the half-saturation constants of the biodegradable hydrocarbons (K$_{gi}$)

262   and λ$_i$. Because these parameters are related to the biodegradation module, we fit the

263   biodegradation module (system of equations (2)) to data obtained from laboratory biodegradation

264   studies cited above. To estimate these values, we used the nonlinear regression function *nlinfit(.)*

265   in MATLAB, which uses the Levenberg-Marquardt algorithm (Moré, 1978), to fit the solution of

266   the biodegradation module to the data. We provided the function with empirical data (see Table 2

267   for sources), the time points at which the data were collected (*X*), our simulated results at *X*, and

268   a random initial guess of parameter values. The system was integrated by calling a function that

269   takes as input the initial parameter values, the time at which the empirical data were collected,

270   and for any given time *X* uses the MATLAB function *ode15s(.)* to perform the integration. The

271   solution of the system obtained from the function was then evaluated at *X*, using the MATLAB

272   function *deval(.)*. We also estimated the 95% confidence intervals of the predicted values by

273   using the MATLAB function *nlparci(.)*. To achieve this, we provided this function with the

274   coefficient estimates, residuals and the estimated coefficient covariance matrix from *nlinfit(.)*.

275   Some of the microbial model parameters used in the simulation, namely μ, r, and θ, were taken

276 from the literature: the units, values and source of these parameters are provided in Table S2. We

277 assume here that no microbes died during laboratory incubation; thus, in fitting the data to our

278 model, we take d to be zero.

2.3.3 Model validation against laboratory data

280 The new stoichiometric model was then validated against CH_4 production data generated in

281 independent but parallel laboratory studies that measured biodegradation of paraffinic diluent in

282 CNUL MFT (Mohamad Shahimin and Siddique, 2017a) and naphtha in Syncrude (Table S1)

283 and CNRL MFT (Mohamad Shahimin and Siddique, 2017b). To this end, the concentrations of

284 the labile hydrocarbons initially present in each diluent were used in the model to predict CH_4

285 production (Table S7). These predictions were compared with measured CH_4 produced by those

286 tailings in independent laboratory experiments using the *goodnessOfFit(.)* function in MATLAB.

287 As input, we provided this function with our test data, the simulated data from our model, and a

288 cost function that determines the goodness of fit. We used the Normalized Mean Square Error

289 (NMSE) function for this statistic, computed as

290 $$\text{NMSE} = 1 - \frac{\|[\text{actual}] - [\text{predicted}]\|^2}{\|[\text{actual}] - [\text{mean of actual}]\|^2},$$

291 where $\|.\|$ indicates the 2-norm of a vector, *predicted* is the output simulated by our model,

292 *actual* is the input test data and *mean of actual* is the mean of the test data. NMSE $\in [-\infty, 1]$

293 where -∞ indicates a bad fit and 1 a perfect fit.

2.4 Quantitative comparison of model prediction and in-situ measurement of CH_4 emissions from OSTP

296 To further validate the applicability of model for predicting in-situ CH_4 emissions, we used (1) a

297 modeling approach where kinetics of CH_4 production were estimated to determine the duration

298 of CH_4 emissions, and (2) a direct approach that yielded a ballpark value of potential CH_4

14

299 emissions. For both approaches, we estimated the total mass of diluent entrained in froth

300 treatment tailings entering Syncrude MLSB, CNRL Horizon and CNUL MRM OSTPs in 2016

301 and 2017 (Table S6) and estimated the mass of individual biodegradable hydrocarbons in diluent

302 (Table S7) using published diluent compositions. To employ the modeling approach, we

303 assumed that these masses of individual hydrocarbons were present at the start of each year (i.e.,

304 the model was run as if all the diluent was introduced on January 1 of the year), while

305 acknowledging the continuous input of similar amounts of diluents in the years preceding 2016.

306 Using the estimated parameter values in Table S4, we modeled CH_4 production and calculated

307 the predicted cumulative CH_4 produced by metabolism of the constituent hydrocarbons over 366

308 days. The model output was compared with cumulative CH_4 emissions measured in flux

309 chambers at the surface of OSTP as reported to the Government of Alberta (unpublished; raw

310 data available upon request) (Table S8). Notably, surface flux measurements of CH_4 are not yet

311 available for the single EPL that was established in 2013, so the current comparison is limited to

312 OSTP measurements. In the direct approach, theoretical CH_4 production was estimated from the

313 masses of individual hydrocarbons biodegraded to methane using stoichiometric equations as

314 described in Table S8.

315 *2.5 Qualitative assessment of model predictions for OSTP and EPL*

In addition to quantitative analyses, the model was also qualitatively challenged to predict the

trajectories of CH_4 generation from OSTP (continuous   ) versus EPL (C_i=0) under

316 hypothetical scenarios of carbon or nitrogen availability in-situ. Phase plane analysis was

317 performed (Supplemental Material section S3) by assuming $C_i^{in}>0$

318

319   that the diluent comprises C_i,

320 i=1,2,3...,18 are identical and sum up to C_T, and that the rate input of all the C_i per unit time

321 into the system is C_T^{in}. Equations were solved for microbial biomass versus total carbon content

322 over time.

323

324

under eight combinations of C_i and N_A limitation

325 The mathematical model and code are available at http://www.judekong.ca/publication/2019-

326 05-01-Methanebiogenesismodel or from the authors upon request. Previous zero- and first-order CH_4 production models from oil sands tailings (Siddique et al.,

3. Results and Discussion

327 2008) used the available limited experimental data for diluent biodegradation and CH_4

328 production from four short-chain *n*-alkanes and four monoaromatic compounds during <1 year

329 incubation with MFT from a single OSTP (Siddique et al., 2007, 2006). Those first

330 approximation models assumed that organic carbon was the sole limiting nutrient in-situ and that

331 microbial biomass was constant in OSTP despite receiving continuous and consistent inputs of

332 diluent in froth treatment tailings. The stoichiometric model described here accounts for

333 additional parameters including recently published biodegradation kinetics and CH_4

334 measurements for 18 relevant hydrocarbons including additional *n*-alkanes and, for the first time,

335 *iso*-alkanes, incubated for much longer (up to 6.5 years) with MFT from three different OSTP

336 impacted by distinct diluents. These additional experimental data allow the estimation of some

337 kinetic parameters not previously considered and enable the new model to account for more

338 biological factors than the previous models, so as to be adaptable to future modeling of in-situ

339 CH_4 production from OSTP and EPL.

340 *3.1 Data fitting to biodegradation and methane generation modules.*

341 The biodegradation module was evaluated by fitting system of equations (2) to published

342 experimental data sets for the 18 labile hydrocarbons listed in Table 2. Figures S3-S5 show the

343 simulated biodegradation of diluent *n*-alkanes, monoaromatics and *iso*-alkanes compared with

344 measured biodegradation of these components. We obtained goodness-of-fit statistics (NMSE)

345 ranging from 0.85-1.00 (Table S3). These statistics show that the performance of the module

346 with respect to the training data is good.

347   To integrate the methane generation module with the biodegradation module, only three

348 model parameters were available in the literature (Table S2); others had to be estimated from

349 experimental data (Tables 2 and S4). Using these calculated values we applied the full

350 stoichiometric model to methane measurements from a suite of experiments analogous to but

351 independent of those used to estimate the parameters. Specifically, the CH_4 measurements were

352 acquired during long-term incubation of MFT samples from Syncrude, CNUL and CNRL with

353 their cognate diluents (Table S1, Siddique et al., 2015, Mohamad Shahimin and Siddique, 2017a,

354 respectively). Figure 1 shows that the model predicted methane generation very well for all three

355 types of MFT over long incubation times (> 4 yr incubation for CNUL and CNRL cultures).

356 Additional modeling of Syncrude MFT with mixtures of *n*-alkane or monoaromatic components

357 of its diluent (rather than whole diluent) also showed very good methane prediction (Fig. S6).

358 *3.2 Model evaluation and comparison to previous models*

359 Goodness-of-fit analysis of the stoichiometric model was calculated using NMSE (Table 3) that

360 showed excellent fit, ranging from $0.81 - 0.98$ for the three combinations of MFT and diluent.

361 These NMSE results indicate that the integrated biodegradation and CH_4 production modules

362 rightly capture the behaviour of independent laboratory cultures and that the stoichiometric

363 model is sufficiently flexible to accommodate different inocula and substrates over long

364 incubation periods.

365   The new stoichiometric model was then compared with the previous zero- and first-order

366 kinetic models, as performed previously (Siddique et al., 2008), using the current data set. To

367 this end, we first estimated the zero- and first-order kinetic model-related parameter values for

368 the labile hydrocarbons that were not considered by Siddique et al. (2008) (Table S5). Figures 1

369 and S6, and Table 3 show that the stoichiometric model provides improved predictions over the

370 previous models for describing CH_4 biogenesis from Syncrude MFT and whole naphtha or its

371 components, and is far superior (matching closely with the measured methane) to the simpler

372 models for the CNUL MFT–paraffinic diluent and for CNRL–naphtha combinations, neither of

373 which were available for the previous modeling study. The improved fit regarding lag time and

374 extent of CH_4 production, and the improved NMSE values suggest that the stoichiometric model,

375 which is based on laboratory cultures, would be useful for modeling in-situ CH_4 production from

376 different OSTP and EPL.

377 *3.3 Quantitative comparison of stoichiometric model predictions to measured*

378 *cumulative CH_4 field emissions*

379 To evaluate the feasibility of applying this model based on laboratory cultures to field emissions

380 of CH_4, we compared the reported measured volumes of CH_4 emitted from the surfaces of

381 OSTPs with cumulative CH_4 masses predicted by our model. Table 4 shows the comparison

382 between the reported measured methane emissions from OSTPs in 2016 and 2017 and the

383 maximum theoretical CH_4 yield predicted by our model based on the estimated diluent entering

384 OSTPs (Table S6) for 2016 and 2017. The stoichiometric model predictions are 50-55 % of the

385 measured emissions from Syncrude MLSB and 77-95% of the measured emissions from CNRL

386 OSTP in both years. For CNUL where paraffinic solvent is used, the model predictions were

387 48% of the measured emissions in 2017 but only 17% of the emissions in 2016. This latter

388 difference may be attributed to markedly greater methane emission data from CNUL OSTP

389 reported in 2016 compared to all other OSTPs (Tables 4 and S5). The overall trend is very clear

18

390 that the model predicted about 50% of emissions from Syncrude and CNUL OSTP and >75% of

391 emissions from CNRL OSTP. This likely reflects the diluent compositions, with only ~40% of

392 fugitive Syncrude and CNRL naphtha diluent being considered labile versus ~60% of CNUL

393 paraffinic diluent, based on the mass of known biodegradable hydrocarbons in the diluents

394 (Table S7).

395   This difference between predicted and measured CH_4 masses suggests that (other than

396 possible inaccuracies associated with field measurements) there are other endogenous carbon

397 sources present in OSTP that support methanogenesis but are not currently accounted for by the

398 model. Such possible sources include (but are not limited to): (1) additional labile diluent

399 hydrocarbons not yet identified in our laboratory incubations and therefore not included in the

400 model; (2) recalcitrant hydrocarbons deposited in previous years (and therefore not included in

401 the annual C_i^{in} model input) that are slowly degraded as the community adapts to residual

402 naphtha after depletion of the labile hydrocarbons in lower strata, e.g., some *iso*-alkanes and

403 cycloalkanes having extremely long lag times or slow degradation rates (e.g., Abu Laban et al.,

404 2015); (3) slowly-degradable metabolites produced historically during incomplete

405 biodegradation of hydrocarbon or from non-hydrocarbon carbon substrates; (4) organic matter

406 associated with clays in oil sands ores (Sparks et al., 2003); (5) minor labile components of

407 bitumen e.g., high molecular weight *n*-alkanes (Oberding and Gieg, 2018); and (6) organic

408 additives used in ore processing and deposited with tailings, e.g., citrate that is used as an

409 amendment in some OSTPs (Foght et al., 2017) and is a potentially large source of unaccounted

410 CH_4 in CNUL MRM. Another explanation for larger masses of measured emissions is the

411 delayed, stochastic release of methane produced years ago from labile HCs that is 'trapped' in

412 lower strata of MFT (Guo, 2009) until (1) suitably-sized and -oriented channels are created (e.g.,

413   by microbial activity, Siddique et al., 2014) and/or (2) cumulative gas voids reach critical

414   buoyancy and rise from deep tailings, and/or (3) MFT strata are disturbed by some physical

415   activity in the pond (e.g., moving deposition pipes, transferring MFT to new pits, etc.) allowing

416   escape of gas.

417   There is an agreement between the model predictions and measured field emissions despite

418   the obvious reasons of discrepancy discussed above. However, additional qualitative factors

419   must be addressed to expand the developed model to in-situ predictions while keeping in mind

420   the inherent differences between laboratory cultures and field operations: (1) cultures are

421   incubated with a single input of hydrocarbons, i.e., in "batch mode" with finite C_i^{in}, whereas the

422   upper strata of OSTP receive ongoing input of diluent, i.e., "continuous mode" where $C_i^{in} > 0$.

423   The laboratory cultures are more analogous to EPL, where $C_i^{in} = 0$ or to the lower strata of OSTP

424   to which fresh diluent deposited at the surface cannot effectively diffuse and where, essentially,

425    $C_i^{in} = 0$. (2) As discussed above, anaerobic biodegradation kinetics are currently available for

426   only 18 hydrocarbons in cultures, whereas additional constituents of whole diluent and possibly a

427   small subset of bitumen constituents may be susceptible to biodegradation in-situ. Restriction of

428   the parameter C_i to the current 18 hydrocarbons would likely cause the model to under-estimate

429   methane production in-situ. Selective depletion of naphtha constituents with depth in OSTP has

430   been observed qualitatively (Figure S2 in Foght et al., 2017) and such information could be used

431   in future to expand the substrate range of the stoichiometric model and better represent in-situ

432   biodegradation. (3) The model currently includes a variable for lag time (λ), the time elapsed

433   between addition of hydrocarbon and appearance of measureable CH_4. In fact, lag times of 5-15

434   years were observed between the inauguration of OSTP and the first observation of ebullition at

435   the pond surface (Foght et al., 2017), likely reflecting the time required for establishment of

436 efficient methanogenic communities. However, this variable is likely relevant only to laboratory

437 studies, due to disruption of the microbial consortia during initiation of the cultures, and to newly

438 established OSTP and EPL when transfer of tailings begins. After onset of CH_4 production,

439 OSTP subsequently do not exhibit any apparent lag phases because of continuous diluent input

440 and $\lambda=0$ in-situ. (4) Small scale culture bottles facilitate release of CH_4 from MFT to the

441 headspace for measurement compared with static deep strata in OSTP and EPL that experience

442 physical retention of GHG as methane voids (Guo, 2009). That is, the model predicts CH_4

443 production based on 100% release from MFT; the proportion of gas released to the pond surface

444 versus that retained under hydraulic pressure in-situ is not a component of the model. (5)

445 Methanogenesis depends completely upon the microbial community composition, which is

446 complex (An et al., 2013) and specific to each OSTP and EPL (Wilson et al., 2016), and may

447 diverge from cultured communities during incubation. Although some diversity data exist both

448 for cultures and various MFT, the model does not include parameters to account for the presence

449 or abundance of 'keystone' microbial species because, in tailings, such species currently are

450 incompletely known or identified. Significant efforts in research and testing would be required to

451 integrate microbial community analysis into any CH_4 model for oil sands operations. (6) Finally,

452 the model does not currently include parameters that reflect potential changes to ore processing

453 or OSTP practices such as subtle alterations in diluent composition, intermittent deposition of

454 chemicals from related processes (e.g., ammonium; Foght et al., 2017), changes in froth

455 treatment water temperature, etc.

456 *3.4 Qualitative test of model prediction*

457 Despite the inferred shortcomings of applying the model to field predictions, and in anticipation

458 of acquiring in-situ measurements to provide parameters for use in future for field modeling, it is

459 possible to conduct a qualitative test of the stoichiometric model to determine whether it predicts

460 expected trajectories under different expected field scenarios, e.g., limiting C_T and/or N_A

461 conditions. Whereas cultures receive hydrocarbons in excess of instantaneous microbial demand

462 at the beginning of incubation, as do the upper strata of active OSTP, labile carbon may become

463 limiting in lower (older) strata of OSTP and eventually in EPL and cultures, where diluent is not

464 replenished. Similarly, cultures initially receive a very small but finite amount of soluble

465 nitrogen and have a headspace of N_2 gas (which may serve as a nitrogen source for tailings

466 microbiota; Collins et al., 2016) but the lower strata of OSTP and EPL have no obvious input of

467 biologically available nitrogen (N_A). Therefore this nutrient (or others, currently unidentified)

468 may become limiting with time. Thus, challenging a model developed using culture data with

469 scenarios reflecting in-situ conditions should reveal the strength of the model. Phase plane

470 analyses of eight forms of potential solutions of the stoichiometric model are shown in Figures

471 S7 and S8 and described in Supplemental Material section S3. The model outputs describe the

472 expected trajectories of OSTP and EPL under carbon and/or nitrogen limitation, solving for

473 biomass and total carbon in the system with time, i.e., the sum of all microbial activity in-situ.

474 The predicted behaviour of OSTP with continuous diluent input differs from EPL with no

475 additional hydrocarbon input, and the effect of limiting nutrient (nitrogen) also changes the

476 ultimate endpoints of biomass and carbon in the two scenarios. These outputs qualitatively

477 support the validity of the model as well as indicating that the stoichiometric model could be

478 used to predict specific OSTP and EPL behaviour, to predict the volumes of 'legacy' CH_4 from

479 OSTP and long-term duration of CH_4 production in-situ (particularly from EPL), and to

480 influence decisions about oil sands reclamation strategies. If additional in-situ model parameters

481 are acquired, the model can be further refined to improve predictive power.

4. Conclusions

The stoichiometric model represents a significant advance over previous zero- and first-order kinetic models, particularly because it predicts well the GHG emissions from different operators using distinct diluents that may support different rates of CH_4 production or may ultimately generate greater CH_4 emissions. Application of the model to in-situ CH_4 production is still hampered by limited experimental data and field measurements; some of these gaps may be alleviated as relevant in-situ data are acquired and when future anaerobic studies provide both evidence for susceptibility of additional hydrocarbons to biodegradation and more precise values for model parameters. The model is sufficiently flexible that additional parameters can be added to the modules as laboratory or field data become available. Until such time, the stoichiometric model should assist regulators and oil sands operators in qualitatively assessing long-term GHG emissions from oil sands tailings deposits and EPL reclamation sites.

Appendix A. Supplementary Material

This manuscript is accompanied by Supplementary Material comprising stability analysis of our System, eight tables (Tables S1-S8) and eight figures (Figure S1-S8).

ACKNOWLEDGMENTS

REFERENCES

504 **REFERENCES**

505 Abu Laban, N., Dao, A., Semple, K., Foght, J., 2015. Biodegradation of C_7 and C_8 iso-alkanes

506   under methanogenic conditions. Environ. Microbiol. 17, 4898–4915.

507 Alberta Energy Regulator, 2019. Electronic resource about oil sands [WWW Document]. URL

508   https://www.aer.ca (accessed 7.10.19).

509 Alberta Greenhouse Gas Report, 2016. Alberta Greenhouse Gas Reporting Program 2012

510   Facility Emissions. Available at: https://open.alberta.ca/dataset/9b11d727-06be-4ade-9ad9-

511   cfea1a559103/resource/43aeec2e-b22f-4cf4-9e1b-

512   561aad633ee8/download/2012reportgreenhousegasemissions-sep2016.pdf (accessed May

513   02, 2019)

514 An, D., Caffrey, S.M., Soh, J., Agrawal, A., Brown, D., Budwill, K., Dong, X., Dunfield, P.F.,

515   Foght, J., Gieg, L.M., Hallam, S.J., Hanson, N.W., He, Z., Jack, T.R., Klassen, J., Konwar,

516   K.M., Kuatsjah, E., Li, C., Larter, S., Leopatra, V., Nesbø, C.L., Oldenburg, T., Pagé, A.P.,

517   Ramos-Padron, E., Rochman, F.F., Saidi-Mehrabad, A., Sensen, C.W., Sipahimalani, P.,

518   Song, Y.C., Wilson, S., Wolbring, G., Wong, M.-L., Voordouw, G., 2013. Metagenomics of

519   Hydrocarbon Resource Environments Indicates Aerobic Taxa and Genes to be

520   Unexpectedly Common. Environ. Sci. Technol. 47, 10708–10717.

521   https://doi.org/10.1021/es4020184

522 Burkus, Z., Wheler, J., Pletcher, S., 2014. GHG emissions from oil sands tailings ponds:

523   Overview and modelling based on fermentable substrates. Alberta Environment and

524   Sustainable Resource Devevelopment. November 2014 https://doi.org/10.7939/R3F188

525 Charette, T., Castendyk, D., Hrynyshyn, J., Kupper, A., McKenna, G., Mooder, B., 2012. End Pit

526   Lakes Guidance Document 2012. Cumulative Environmental Management Association Fort

527   McMurray, Alberta, Canada 2010. http://library.cemaonline.ca/ckan/dataset/2010-

528   0016/resour ce/1632ce6e-d1a0-441a-a026-8a839f1d64bc (accessed 4.28.19).

529 Collins, C.E.V., 2013. Methane Production in Oil Sands Tailings under Nitrogen-Depleted

530   Conditions. Master's thesis. University of Alberta.

531 Collins, C.E.V., Foght, J.M., Siddique, T., 2016. Co-occurrence of methanogenesis and N 2

532   fixation in oil sands tailings. Sci. Total Environ. 565, 306–312.

533 Foght, J.M., Gieg, L.M., Siddique, T., 2017. The microbiology of oil sands tailings: Past,

534   present, future. FEMS Microbiol. Ecol. 93 (5), fix034 https://doi.org/10.1093/femsec/fix034

535 Government of Alberta, 2019a. Electronic resource about oil sands [WWW Document]. URL

536   https://www.energy.alberta.ca/OS/AOS/Pages/default.aspx (accessed 4.24.19).

537 Government of Alberta, 2019b. Oil Sands Information Portal [WWW Document]. URL

538   http://osip.alberta.ca/map/ (accessed 7.14.19).

539 Guo, C., 2009. Rapid densification of the oil sands mature fine tailings (MFT) by microbial

540   activity. PhD thesis, University of Alberta. https://doi.org/10.7939/R3K988

541 Makino, W., Cotner, J.B., Sterner, R.W., Elser, J.J., 2003. Are bacteria more like plants or

542   animals? Growth rate and resource dependence of bacterial C: N: P stoichiometry. Funct.

543   Ecol. 17, 121–130.

544 Mohamad Shahimin, M.F., Foght, J.M., Siddique, T., 2016. Preferential methanogenic

545   biodegradation of short-chain n-alkanes by microbial communities from two different oil

546   sands tailings ponds. Sci. Total Environ. 553, 250–257.

547 Mohamad Shahimin, M.F., Siddique, T., 2017a. Methanogenic biodegradation of paraffinic

548   solvent hydrocarbons in two different oil sands tailings. Sci. Total Environ. 583, 115–122.

549 Mohamad Shahimin, M.F., Siddique, T., 2017b. Sequential biodegradation of complex naphtha

550   hydrocarbons under methanogenic conditions in two different oil sands tailings. Environ.

551   Pollut. 221, 398–406.

552   Moré, J.J., 1978. The Levenberg-Marquardt algorithm: implementation and theory. In G. A.

553   Watson, (Ed.), *Numerical Analysis*, Lecture Notes in Mathematics 630. Springer, pp. 105–

554   116.

555   Oberding, L.K., Gieg, L.M., 2018. Methanogenic paraffin biodegradation: alkylsuccinate

556   synthase gene quantification and dicarboxylic acid production. Appl. Environ. Microbiol.

557   84(1), e01773-17. https://doi.org/10.1128/AEM.01773-17.

558   Penner, T.J., Foght, J.M., 2010. Mature fine tailings from oil sands processing harbour diverse

559   methanogenic communities. Can. J. Microbiol. 56, 459–470. https://doi.org/10.1139/W10-

560   029

561   Risacher, FF; Morris, PK; Arriagaa, D.; Goada, C; Colenbrander Nelson, T.; Slater, GF; Warren,

562   LA. 2018. The interplay of methane and ammonia as key oxygen consuming constituents in

563   early stage development of Base Mine Lake, the first demonstration oil sands pit lake. Appl.

564   Geochem. 93, 49–59 https://doi.org/10.1016/j.apgeochem.2018.03.013

565   Roberts, D.J., 2002. Methods for assessing anaerobic biodegradation potential. In: Hurst, C.J.,

566   Crawford, R.L., Knudson, G.R., McInerney, M.J., Stetzenbach, L.D. (Eds.), Manual of

567   Environmental Microbiology, second ed. ASM Press, USA, pp.1008–1017.

568   Siddique, T., Fedorak, P.M., Foght, J.M., 2006. Biodegradation of short-chain n-alkanes in oil

569   sands tailings under methanogenic conditions. Environ. Sci. Technol. 40, 5459–5464.

570   Siddique, T., Fedorak, P.M., MacKinnon, M.D., Foght, J.M., 2007. Metabolism of BTEX and

571   naphtha compounds to methane in oil sands tailings. Environ. Sci. Technol. 41, 2350–2356.

572   Siddique, T., Gupta, R., Fedorak, P.M., MacKinnon, M.D., Foght, J.M., 2008. A first

573   approximation kinetic model to predict methane generation from an oil sands tailings

574   settling basin. Chemosphere 72, 1573–1580.

575 Siddique, T., Kuznetsov, P., Kuznetsova, A., Arkell, N., Young, R., Li, C., Guigard, S.,

576   Underwood, E., Foght, J.M., Raymond, J., Grunden, A.M., 2014. Microbially-accelerated

577   consolidation of oil sands tailings. Pathway I: changes in porewater chemistry. Front.

578   Microbiol. 5, 106. https://doi.org/10.3389/fmicb.2014.00106

579 Siddique, T., Mohamad Shahimin, M.F., Zamir, S., Semple, K., Li, C., Foght, J.M., 2015. Long-

580   term incubation reveals methanogenic biodegradation of C_5 and C_6 iso-alkanes in oil sands

581   tailings. Environ. Sci. Technol. 49, 14732–14739.

582 Siddique, T., Penner, T., Semple, K., Foght, J.M., 2011. Anaerobic biodegradation of longer-

583   chain *n*-alkanes coupled to methane production in oil sands tailings. Environ. Sci. Technol.

584   45, 5892–5899.

585 Siddique, T., Stasik, S., Mohamad Shahimin, M.F., Wendt-Potthoff, K., 2018. Microbial

586   communities in oil sands tailings: their implications in biogeochemical processes and

587   tailings management. Springer Nat. Switz. AG 2018 T. J. McGenity (ed.), Microbial

588   Communities Utilizing Hydrocabons and Lipids: Handbook of Hydrocarbon and Lipid

589   Microbiology, 2nd edn. Springer, Cham, 1-33.

590 Sparks, B.D., Kotlyar, L.S., O'Carroll, J.B., Chung, K.H., 2003. Athabasca oil sands: effect of

591   organic coated solids on bitumen recovery and quality. J. Pet. Sci. Eng. 39, 417–430.

592 Sterner, R.W., Elser, J.J., 2002. Ecological stoichiometry: the biology of elements from

593   molecules to the biosphere. Princeton University Press.

594 Symons, G.E., Buswell, A.M., 1933. The methane fermentation of carbohydrates1, 2. J. Am.

595   Chem. Soc. 55, 2028–2036.

596   Wilson, S.L., Li, C., Ramos-Padrón, E., Nesbø, C., Soh, J., Sensen, C.W., Voordouw, G., Foght,

597   J., Gieg, L.M., 2016. Oil sands tailings ponds harbour a small core prokaryotic microbiome

598   and diverse accessory communities. J. Biotechnol. 235, 187–196.

599   https://doi.org/10.1016/j.jbiotec.2016.06.030

600

601   **Table 1:** Definition of terms used in model development

Term	Definition
C_i	mass of individual labile hydrocarbons in the system, where $i=1\ldots n$, assuming n labile hydrocarbons in system *
C_i^{in}	mass of C_i inflow to the system
C_T	total mass of labile (biodegradable) hydrocarbon in the system (i.e., the sum of all C_i)
μ	specific microbial growth rate of microbes (bacteria and archaea) supported by C_T
μ_i	specific microbial growth rate supported by each labile hydrocarbon C_i
N_T	total mass of nitrogen in the system
N_A	mass of N_T that is biologically available §
B	total biomass of living microbes
b	biomass of dead microbes
β_i	the proportion of C_i contained in dead biomass that is available for microbial recycling
θ	the ratio of nitrogen to carbon associated with microbial biomass B
r	proportionality constant defining efficiency of conversion of C_T to B
r_i	proportionality constant defining efficiency of conversion of each C_i to B; r_i = B / C_i consumed
λ_i	lag period before the onset of biodegradation of each C_i
d	microbial cell death rate
K_f	N_A-dependent half-saturation constant
K_{gi}	C_i-dependent half-saturation constant
Γ_i	expected yield of CH_4 from biodegradation of one mole of C_i
G_i	Total CH_4 and CO_2 generated from the biodegradation of C_i
η	fraction of sum of Γ_i for all i, yielded by biodegradation of C_T; i.e., methane bioconversion efficiency factor
η_i	fraction of Γ_i yielded by biodegradation of each C_i

602   *, in developing the current model, we considered 18 specific hydrocarbons present in naphtha
603   and paraffinic diluents (see Table 2)
604   §, e.g., nitrate, nitrite, ammonium, dinitrogen (N_2 gas), labile organic N compounds (e.g.,
605   macromolecules in biomass), but not complex molecules (e.g., resins found in bitumen)

Table 2: List of 18 labile diluent hydrocarbons used in model development, sources of data and type of tailings used to generate data for the biodegradation module and to estimate model parameter values, and the model parameters estimated using those data (see Table S4 for parameter definitions and values).

Hydrocarbon	Source of data	Type of tailings	Parameters estimated from the data
n-Alkanes			
C_5	Mohamad Shahimin et al. (2016)	CNUL	$K_{g_{C_5}}$ and C_5-lag
C_6, C_7, C_8, C_{10}	Siddique et al. (2006)	Syncrude	B(0), K_f, N_T, $K_{g_{C_6}}$, $K_{g_{C_7}}$, $K_{g_{C_8}}$, $K_{g_{C_{10}}}$, C_6-lag, C_7-lag, C_8-lag and C_{10}-lag.
C_9	Table S1	Syncrude	$K_{g_{C_9}}$ and C_9-lag
iso-Alkanes *			
2-MC$_6$[§], 3-MC$_6$, 2-MC$_7$, 4-MC$_7$, 2-MC$_8$, 3-MC$_8$[§], 2-MC$_9$[§],	Siddique et al., unpublished	Syncrude	$K_{g_{3-MC_6}}$, $K_{g_{2-MC_7}}$, $K_{g_{4-MC_7}}$, $K_{g_{2-MC_8}}$, 3-MC$_6$–lag, 2-MC$_7$-lag, 4-MC$_7$-lag, and 2-MC$_8$-lag
2-MC$_5$	Mohamad Shahimin and Siddique (2017a)	CNUL	$K_{g_{2-MC_5}}$ and 2-MC$_5$-lag
Monoaromatics			
Toluene, *o*-Xylene, *m*- plus *p*-Xylene	Siddique et al. (2007)	Syncrude	$K_{g_{toluene}}$, $K_{g_{o-xylene}}$, $K_{g_{mp-xylene}}$, toluene-lag, *o*-xylene-lag, and *m,p*-xylene-lag

* M denotes a methyl group; i.e., 2-MC$_6$ is 2-methylhexane, etc. See Methods section 2.3.1 for full list of abbreviations

§ The values of model parameters K_g and lag for 2-MC$_6$, 3-MC$_8$ and 2-MC$_9$ are not available from empirical studies and are assumed to be the same as those for 3-MC$_6$, 2-MC$_8$ and 2-MC$_8$, respectively, due to their similar molecular weights.

617   **Table 3**: Normalized mean square error (NMSE) analysis of model predictions and measured
618   CH_4 production from laboratory cultures comprising three MFT samples incubated with their
619   cognate diluents. The zero- and first-order models were implemented as described by Siddique et
620   al. (2008) using data reported in the current study. See Figures 1 and S6 for graphical
621   comparison of model outputs.

	NMSE values		
	MFT source and diluent type		
	Syncrude	**CNUL**	**CNRL**
Model	**Naphtha diluent**	**Paraffinic diluent**	**Naphtha diluent**
Zero-order	-0.28	-1.00	-1.10
First-order	-0.65	0.82	0.61
Stoichiometric	0.81	0.98	0.97

622

623 **Table 4:** Comparison of cumulative field measurements of CH_4 emissions in 2016 and 2017 in
624 three OSTP versus stochiometric model predictions of cumulative in-situ CH_4 emissions from
625 those OSTP.

| Operator and OSTP (date)	Field measurements of CH_4 emissions (moles x 10^6) *	Stochiometric model predictions of methane emissions (moles x 10^6)	Proportion of field emissions predicted by model (%) §
Syncrude MLSB (2016)	1191	656	55
Syncrude MLSB (2017)	991	492	50
CNRL Horizon (2016)	336	321	95
CNRL Horizon (2017)	599	459	77
CNUL MRM (2016)	2634	445	17
CNUL MRM (2017)	1051	506	48

626 * Unpublished surface flux measurements (Government of Alberta; raw data available upon
627 request), reported as tonnes and converted to moles at standard temperature and pressure

628 § for detailed calculations see Table S8

FIGURE LEGEND

630 **Figure 1**: Comparison of CH_4 production predicted by the stoichiometric model versus CH_4

631 measured in laboratory cultures independent of those used to generate the stoichiometric model

632 and parameters (Table S4). Methane measurements (diamond symbols) are from cultures

633 comprising: (A), Syncrude MFT incubated with its naphtha diluent (B), CNUL MFT incubated

634 with its paraffinic diluent; and (C), CNRL MFT incubated with its naphtha diluent. Solid lines

635 represent the stoichiometric model prediction; dashed lines and dotted lines respectively

636 represent predictions made by applying the previous zero-order and first-order models

637 (Siddique et al., 2008) to the independent data set.   The parameters values used in simulating

638 the zero-order and first-order models were obtained from Siddique et al. (2008) and Table S5.
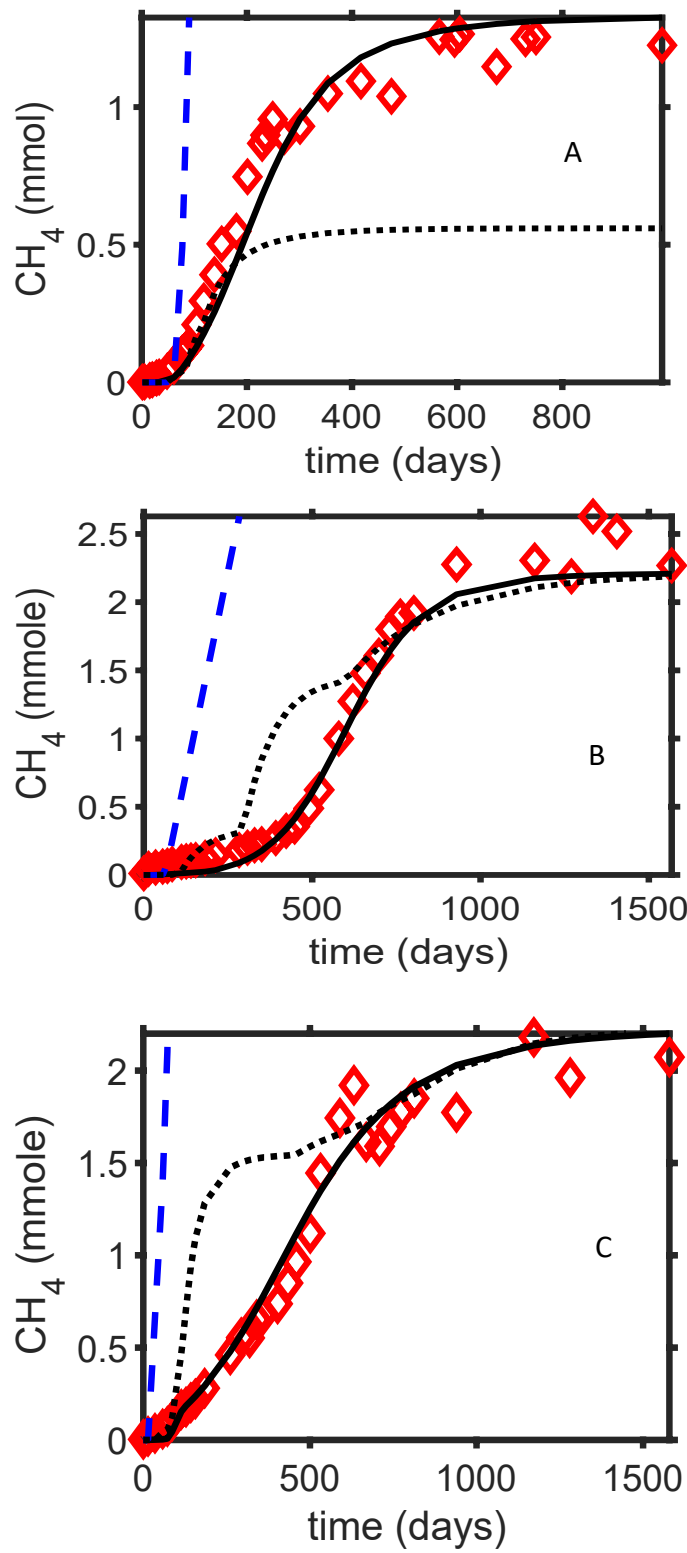
639
640
641   **Figure: 1**

Appendix A:

Second-generation stoichiometric mathematical model to predict methane emissions from oil sands tailings

Jude Kong[1,2], Hao Wang[2*†], Tariq Siddique[3*‡], Julia Foght[4], Kathleen Semple[4], Zvonko Burkus[5],

and Mark Lewis[2,4]

[1]Center for Discrete Mathematics and Theoretical computer Science, Rutgers University, 96

Frelinghuysen Road Piscataway, NJ 08854-8018, USA

[2]Department of Mathematical and Statistical Sciences, University of Alberta, Edmonton, AB T6G 2G1,

Canada

[3]Department of Renewable Resources, University of Alberta, Edmonton, AB T6G 2G7, Canada

[4]Department of Biological Sciences, University of Alberta, Edmonton, AB T6G 2E9, Canada

[5]Alberta Environment and Parks, Government of Alberta, Edmonton, Canada

Corresponding authors' emails:

[*†] Mathematical approach (Hao Wang); hao8@ualberta.ca

[*‡] Biological approach (Tariq Siddique); tariq.siddique@ualberta.ca

The following Supplementary Material contains the mathematical analysis of the system of

equations (2), eight tables (Tables S1- S8) and eight figures (Figures S1-S8).

662 # S1. Brief description of MFT laboratory culture methods used to generate
663 data for model development and testing

664 Details of laboratory culture preparation can be found in published papers (Mohamad Shahimin

665 et al., 2016; Mohamad Shahimin and Siddique, 2017a, 2017b, Siddique et al., 2007, 2006).

666 Briefly and very generally, bulk samples of MFT were dispensed anaerobically into small serum

667 bottles (microcosms) in replicate (typically triplicates) amended with an equal volume of sterile

668 methanogenic medium comprising inorganic salts, trace vitamins, a redox indicator and sulfide

669 as a reducing agent, but lacking organic carbon, and sealed under an atmosphere of 80% O_2-free

670 N_2, balance CO_2. The microcosms were allowed to incubate stationary in the dark at room

671 temperature (ca. 22°C) for 2 weeks to acclimate, then the headspace was flushed with O_2-free N_2

672 plus CO_2 to remove any CH_4 produced from endogenous substrates. The microcosms were then

673 amended by injecting neat diluent supplied by the operator, or in one case defined mixtures of

674 pure hydrocarbon constituents of the diluent (i.e., mixtures of *n*-alkanes or monoaromatics;

675 Figure S6). During incubation headspace gases were sub-sampled at intervals for analysis by gas

676 chromatography to determine cumulative CH_4 production. Likewise the MFT slurry was sub-

677 sampled at intervals to analyze residual hydrocarbons using gas chromatography with mass

678 spectrometry and thereby to calculate biodegradation by difference. Control microcosms

679 containing MFT that had been heat-sterilized using an autoclave were included with each

680 experiment to account for any abiotic losses of hydrocarbons.

681 ## S2. Model development details

682 ### *S2.1 Mathematical analysis of the biodegradation module*

683 Here, a basic mathematical analysis of the system of equations (2) is provided. First we let C_T to

684 represent the sum of all the labile hydrocarbons in the system and the sum of all C_i^{in} to be C_T^{in}..

685 We assume that $\lambda_i = 0,$ for all i=1,2,3..n. This leads to a system of two differential equations.

686   To simplify our phase plane analysis in a meaningful way, we adjusted the second differential by

687   introducing a new variable:

688   $A = \frac{B}{r} + C_T$. 'A' represents the sum of the total carbon available in the system and bacterial

689   biomass. We assume that f, g are linear and find their linear approximations:

690
$$f(N_T - \theta B) \approx f(0) + f'(0)(N_T - \theta B)$$

691
$$\Rightarrow f(N_T - \theta B) \approx \frac{N_T - \theta B}{K_f}$$

692
$$g\left(A - \frac{B}{r}\right) \approx g(0) + g'(0)\left(A - \frac{B}{r}\right)$$

693
$$\Rightarrow g\left(A - \frac{B}{r}\right) \approx \frac{A - \frac{B}{r}}{K_g}$$

694   We thus have the following system in which only one of the two differential equations has a

695   minimum function, greatly simplifying the analysis:

696
$$\dot{A} = \frac{r-1}{r} dB + C_T^{in} = F(B) \qquad\qquad (S1)$$

698
$$\dot{B} = \mu B min\left\{f(N_T - \theta B), g\left(A - \frac{B}{r}\right)\right\} - dB = BG(A, B).$$

697

699   Next, we look at the stability analysis of the system. For this purpose, we construct a phase plane

700   of the system, (i.e. a graph of the solution trajectories mapped out by points *(A(t),B(t))* as t varies

701   over $(\infty, +\infty)$) in order to identify the steady state solutions. We call $F(B) = 0$ and $G(A, B) = 0$

702   (the lines on which trajectories are horizontal or vertical) the nullclines of system of equations

703   (S1). The steady state solutions are the points where the nullclines (but not different branches of

704   the same nullcline) cross each other. For the stability of the steady states, we compute the

705   Jacobian matrix corresponding to each equilibrium point $J(A^*, B^*)$, where (A^*, B^*) is a given

706   equilibrium point. We use the sign of the trace and determinant of $J(A^*, B^*)$ to determine the

707   nature of the given equilibrium point. Let $D = \det J(A^*, B^*)$ and $T_r = \operatorname{trace} J(A^*, B^*)$. Note that:

708   1) If $D < 0$, the eigenvalues of $J(A^*, B^*)$ are real and of opposite signs, and the phase

709   portrait is a saddle (which is always unstable).

710   2) If $0 < D < \frac{T_r^2}{4}$, the eigenvalues of $J(A^*, B^*)$ are real, distinct, and of the same sign, and

711   the phase portrait is a node, stable if $T_r < 0$ and unstable if $T_r > 0$.

712   3) If $0 < T_r^2 < D$, the eigenvalues of $J(A^*, B^*)$ are neither real nor purely imaginary, and

713   the phase portrait is a spiral, stable if $T_r < 0$ and unstable if $T_r > 0$. Using this idea, we

714   carried out the analysis as follows:

715

716   ***S2.2 Stability Analysis of OSTP system ($C_T^{in} \neq 0$)***

717   **Steady states:**

718   **A-Nullclines**:

719    $\dot{A} = 0, \implies B = \dfrac{rC_T^{in}}{d(1-r)}.$

720   **B-Nullclines:**

721    $$\dot{B} = 0, \implies B = 0 \ or \ G(A, B) = 0.$$

722    $$G(A, B) = 0, \implies \begin{cases} B = Ar - \dfrac{dk_g r}{\mu} \ if \ \dfrac{N_T - \theta B}{k_f} > \dfrac{A - \dfrac{B}{r}}{k_g} \\ B = \left(N_T - \dfrac{dk_f}{\mu} \right) \dfrac{1}{\theta} \ if \ \dfrac{N_T - \theta B}{k_f} < \dfrac{A - \dfrac{B}{r}}{k_g} \end{cases}$$

723   **Case 1:** Suppose $\theta - \dfrac{k_f}{k_g r} > 0$, then

724
$$G(A,B) = 0, \Longrightarrow \begin{cases} B = Ar - \dfrac{dk_g r}{\mu} \ if \ B < \left(N_T - \dfrac{Ak_f}{k_g}\right)\left(\dfrac{k_g r}{\theta k_g r - k_f}\right) \\ B = \left(N_T - \dfrac{dk_f}{\mu}\right)\dfrac{1}{\theta} \ if \ B > \left(N_T - \dfrac{Ak_f}{k_g}\right)\left(\dfrac{k_g r}{\theta k_g r - k_f}\right) \end{cases}$$

725

726 **Case 1.1:** If $C_T^{in} > \dfrac{d(1-r)}{r\theta}\left(N_T - \dfrac{dk_f}{\mu}\right)$, there will be no intersection between the A and B-

727 nullclines as shown in Panel A of Figure S7. Hence the system will have no equilibrium point.

728

729 **Case 1.2:** If $C_T^{in} < \dfrac{d(1-r)}{r\theta}\left(N_T - \dfrac{dk_f}{\mu}\right)$, the two nullclines will intersect at one unique point $E_1 =$

730 $\left(\dfrac{\mu c^{in} + d^2 k_g(1-r)}{d(1-r)\mu}, \dfrac{rC_T^{in}}{d(1-r)}\right)$ as shown in Panel B of Figure S7. Hence if

731 $C_T^{in} < \dfrac{d(1-r)}{r\theta}\left(N_T - \dfrac{dk_f}{\mu}\right)$, the system will have a unique internal equilibrium point E_1.

732

733 **Case 1.3:** If $C_T^{in} = \dfrac{d(1-r)}{r\theta}\left(N_T - \dfrac{dk_f}{\mu}\right)$, the two nullclines will intersect on the line

734 $\left\{\left(A, \left(T - \dfrac{dk_f}{\mu}\right)\dfrac{1}{\theta}\right) : A > \dfrac{1}{r}\left[\left(T - \dfrac{dk_f}{\mu}\right)\dfrac{1}{\theta} + \dfrac{dk_g r}{\mu}\right]\right\}$ as can be seen in Panel A of Figure S8.

735 Consequently, If $C_T^{in} = \dfrac{d(1-r)}{r\theta}\left(N_T - \dfrac{dk_f}{\mu}\right)$, the system will have an infinite number of

736 equilibrium points $E_2 = \left\{\left(A, \left(N_T - \dfrac{dk_f}{\mu}\right)\dfrac{1}{\theta}\right) : A > \dfrac{1}{r}\left[\left(N_T - \dfrac{dk_f}{\mu}\right)\dfrac{1}{\theta} + \dfrac{dk_g r}{\mu}\right]\right\}$

737

738 **Case 2:** Suppose $\theta - \dfrac{k_f}{k_g r} < 0$, then

739
$$G(A,B) = 0, \Longrightarrow \begin{cases} B = Ar - \dfrac{dk_g r}{\mu} \ if \ B > \left(N_T - \dfrac{Ak_f}{k_g}\right)\left(\dfrac{k_g r}{\theta k_g r - k_f}\right) \\ B = \left(N_T - \dfrac{dk_f}{\mu}\right)\dfrac{1}{\theta} \ if \ B < \left(N_T - \dfrac{Ak_f}{k_g}\right)\left(\dfrac{k_g r}{\theta k_g r - k_f}\right). \end{cases}$$

740

741   Note that the slope of the line $B = Ar - \frac{dk_g r}{\mu}$ is less than that of $B = \left(N_T - \frac{Ak_f}{k_g}\right)\left(\frac{k_g r}{\theta k_g r - k_f}\right)$,

742   since $\frac{k_f}{k_f - \theta k_g r} > 1$. Therefore, the point where the line $B = Ar - \frac{dk_g r}{\mu}$ intersects the A-axis, $\frac{dk_g}{\mu}$,

743   must be less than $\frac{Tk_g}{k_f}$, the point where the $B = \left(N_T - \frac{Ak_f}{k_g}\right)\left(\frac{k_g r}{\theta k_g r - k_f}\right)$ intersect the A-axis, for

744   the two lines to intersect on the first quadrant.

745

746   **Case 2.1:** If $C_T^{in} > \frac{d(1-r)}{r\theta}\left(N_T - \frac{dk_f}{\mu}\right)$, as with Case 1.1, there will be no intersection between

747   the A and B-nullclines as shown in Panel B of Figure S8. Hence the system will have no

748   equilibrium point.

749

750   **Case 2.2:** $C_T^{in} < \frac{d(1-r)}{r\theta}\left(N_T - \frac{dk_f}{\mu}\right)$, the two nullclines will intersect at one unique point $E_3 =$

751     $\left(\frac{\mu C^{in} + d^2 k_g (1-r)}{d(1-r)\mu}, \frac{r C_T^{in}}{d(1-r)}\right)$ as shown in Panel C of Figure S8. Hence if $\theta \, C_T^{in} < \frac{d(1-r)}{r\theta}\left(N_T - \frac{dk_f}{\mu}\right)$,

752   the system will have a unique internal equilibrium point E_3.

753

754   **Case 2.3:** If $C_T^{in} = \frac{d(1-r)}{r\theta}\left(N_T - \frac{dk_f}{\mu}\right)$, the two nullclines will intersect on the line

755     $\left\{\left(A, \left(N_T - \frac{dk_f}{\mu}\right)\frac{1}{\theta}\right) : A > \frac{1}{r}\left[\left(N_T - \frac{dk_f}{\mu}\right)\frac{1}{\theta} + \frac{dk_g r}{\mu}\right]\right\}$ as shown in Panel D of Figure S8. Thus, If

756     $C_T^{in} = \frac{d(1-r)}{r\theta}\left(N_T - \frac{dk_f}{\mu}\right)$, the system will have an infinite number of equilibrium points $E_4 =$

757     $\left\{\left(A, \left(N_T - \frac{dk_f}{\mu}\right)\frac{1}{\theta}\right) : A > \frac{1}{r}\left[\left(N_T - \frac{dk_f}{\mu}\right)\frac{1}{\theta} + \frac{dk_g r}{\mu}\right]\right\}$

758

759   Thus an OSTP system may have 0, 1, or an infinite number of equilibrium points depending on

760   the volume of fresh labile hydrocarbons input into the system, C_T^{in}. If $C_T^{in} > \frac{d(1-r)}{r\theta}\left(N_T - \right.$

761     $\left. \frac{dk_f}{\mu}\right)$, the system will have no equilibrium point; if $C_T^{in} < \frac{d(1-r)}{r\theta}\left(N_T - \frac{dk_f}{\mu}\right)$, it will have one

762   unique equilibrium point , $\left(\frac{\mu C_T^{in} + d^2 k_g(1-r)}{d(1-r)\mu}, \frac{rC_T^{in}}{d(1-r)}\right)$; and if $\frac{rC_T^{in}}{d(1-r)} = \left(N_T - \frac{dk_f}{\mu}\right)\frac{1}{\theta}$, it will have an

763   infinite number of equilibrium points given by $\left\{\left(A, \left(N_T - \frac{dk_f}{\mu}\right)\frac{1}{\theta}\right) : A > \frac{1}{r}\left[\left(N_T - \frac{dk_f}{\mu}\right)\frac{1}{\theta} + \right.\right.$

764     $\left.\left.\frac{dk_g r}{\mu}\right]\right\}$.

765

766   ***S2.2.1 Stability of equilibrium points in OSTP scenario:***

767   To determine the local stability of the equilibria above, we consider the Jacobian matrix of

768   System of equations (S1),

769
$$J(A, B) = \begin{pmatrix} 0 & \dfrac{(r-1)d}{r} \\ BG_A(A,B) & G(A,B) + BG_B(A,B) \end{pmatrix} \quad (S1.)$$

770   Where

772
$$G(A, B) = \begin{cases} \dfrac{\mu\left(A - \dfrac{B}{r}\right)}{k_g} - d \ if \ \dfrac{N_T - \theta B}{k_f} > \dfrac{A - \dfrac{B}{r}}{k_g} \\ \dfrac{\mu(N_T - \theta B)}{k_f} - d \ if \ \dfrac{N_T - \theta B}{k_f} < \dfrac{A - \dfrac{B}{r}}{k_g}, \end{cases}$$

773
$$G_A(A, B) = \begin{cases} \dfrac{\mu}{k_g} \ if \ \dfrac{N_T - \theta B}{k_f} > \dfrac{A - \dfrac{B}{r}}{k_g} \\ 0 \ if \ \dfrac{N_T - \theta B}{k_f} < \dfrac{A - \dfrac{B}{r}}{k_g} \end{cases}$$

771   and

$$G_B(A,B) = \begin{cases} \dfrac{-\mu}{k_g} & if \ \dfrac{N_T - \theta B}{k_f} > \dfrac{A - \dfrac{B}{r}}{k_g} \\[4mm] \dfrac{-\theta}{k_f} & if \ \dfrac{N_T - \theta B}{k_f} < \dfrac{A - \dfrac{B}{r}}{k_g} \end{cases}$$

Stability of E_1:

$$J(E_1) = \begin{pmatrix} 0 & \dfrac{(r-1)d}{r} \\[4mm] \dfrac{\mu r C_T^{in}}{k_g d(1-r)} & \dfrac{-C_T^{in}\mu}{d(1-r)k_g} \end{pmatrix} \quad (S2.)$$

Since $det\big(J(E_1)\big) = \dfrac{\mu C_T^{in}}{k_g}$ is greater than zero and $T_r\big(J(E_1)\big) = \dfrac{-C_T^{in}\mu}{d(1-r)k_g} < 0$, this implies that

both eigenvalues of $J(E_1)$ have negative real parts. Hence E_1 is a locally stable equilibrium

point. It is easy to see that E_1 is a stable spiral.

Stability of E_2:

$$J(E_2) = \begin{pmatrix} 0 & \dfrac{(r-1)d}{r} \\[4mm] 0 & \dfrac{-r C_T^{in}\mu\theta}{d(1-r)k_f} \end{pmatrix} \quad (S3.)$$

$det\big(J(E_2)\big) = 0$ and $T_r\big(J(E_2)\big) = \dfrac{-r C_T^{in}\mu\theta}{d(1-r)k_f} < 0$.

Since the $T_r\big(J(E_2)\big)$ is negative and $det\big(J(E_2)\big)$ is zero, one eigenvalue is zero and the other is

negative. Thus E_2 is a line of locally asymptotically stable equilibrium points. Hence both the

788   internal equilibrium point E_1 and the line of equilibrium points E_2 are locally asymptotically

789   stable.

790

791   ***S2.2.2 End pit lake scenario ($C_T^{in} = 0$):***

792   **Steady states:**

793   ***A*-Nullclines:**

794
$$\dot{A} = 0 \implies B = 0$$

795   ***B*-Nullclines:**

796
$$\dot{B} = 0 \implies B = 0 \; or \; G(A, B) = 0.$$

797

798   Panels C and D of Figure S7 show that, irrespective of the slope of the line $B = Ar - \frac{dk_g r}{\mu}$, the

799   A-and B-nullclines have an infinite number of intersections, given by

800    $E_5 = \{(A, 0) : A \geq 0\}$. Thus for $C_T^{in} = 0$, system of equations (S1) has an infinite number of

801   equilibrium points given by E_5.

802

803   **Stability of E_5:**

804
$$J(E_5) = \begin{pmatrix} 0 & \dfrac{(r-1)d}{r} \\ 0 & \dfrac{\mu A}{k_g} - d \end{pmatrix} \quad (4.)$$

805    $det\big(J(E_5)\big) = 0$ and $T_r\big(J(E_5)\big) = \frac{\mu A}{k_g} - d$. If $A < \frac{dk_g}{\mu}$, $T_r(J(E_5))$ will be less than zero and hence

806   E_5 will be asymptotically stable. On the other hand, if $A \geq \frac{dk_g}{\mu}$, then $T_r(J(E_5))$ will be greater

807   than 0 and thus E_5 will be a line of unstable equilibrium points.

S3. Qualitative challenge of model prediction

808

809   Figures S7 and S8 show eight theoretical in-situ scenarios presented as phase plane

810   diagrams showing solutions for microbial biomass versus total carbon content (both unitless)

811   under conditions of carbon or nitrogen limitation. The directional arrows account for time,

812   nullclines define the vector fields, and nullcline intersections (fixed points) indicate regions

813   where trajectories are horizontal or vertical; i.e., steady states. Panels S7A, S7B and S8A-S8D

814   are relevant to the upper strata of OSTP where the input of labile hydrocarbon is continuous (i.e.

815    $C_T^{in} > 0$) whereas Panels S7C and S7D represent an established EPL where labile carbon (as

816   partially biodegraded diluent) enters the system with deposited MFT but is not replenished (i.e.,

817    $C_T^{in} = 0$) Furthermore, the availability of nitrogen (N_A) differs for each panel, as described

818   below.

819   Let C_0^{in}, C_1^{in} and C_2^{in} denote sums of labile hydrocarbons with values $\left(N_T - \frac{dk_f}{\mu}\right)\frac{d(1-r)}{\theta r}$,

820    $\left(\frac{C_T^{in}}{d(1-r)} + \frac{dK_g}{\mu}\right)$ and $\frac{1}{r}\left[\left(T - \frac{dk_f}{\mu}\right)\frac{1}{\theta} + \frac{dk_g r}{\mu}\right]$ respectively. Also, let B_0 and B_1 denote two

821   different values of bacterial biomass. $B_0 = \left(N_T - \frac{dk_f}{\mu}\right)\frac{1}{\theta}$ and $B_1 = \frac{d(1-r)}{\theta r}$. Figures S7A and S8B

822   show the predicted behaviour of OSTP in which the rate of input of hydrocarbons into the OSTP

823   per unit time is $> C_0^{in}$. In this scenario, biomass moves towards B_0 (i.e., steady state). As

824   biomass stabilizes, nitrogen becomes the limiting factor in microbial growth and thus bacteria

825   consume only the amount of hydrocarbon permitted by N_A. This leads to a accumulation of

826   hydrocarbon in the system due to the continuous influx of diluent and inability of bacteria to

827   degrade all the carbon input. Such a scenario would require addition of N_A to the ponds to

828   achieve additional diluent consumption, if that was the management goal. Conversely, restricting

829   N_A in the pond should decrease CH_4 and CO_2 emissions although the potential for gas biogenesis

830 would persist for an indefinite period. Figures S7B and S8D illustrates the case of an OSTP

831 where the rate of input of hydrocarbons into the OSTP per unit time is $< C_0^{in}$. In this case,

832 biomass moves to a value of B_1 and total C_T^{in} moves to C_1^{in}. Because the total labile hydrocarbon

833 deposited into the pond per unit time C_T^{in} is $< C_0^{in}$, carbon becomes the limiting factor for

834 bacterial growth. Thus, biomass will increase to achieve a steady state at which carbon intake is

835 maximized and all C_T is degraded as it enters the system. This scenario requires a continuous

836 (but currently undiscovered) source of N_A in the tailings or the addition of exogenous N_A, i.e., as

837 a management practice. The final possible scenario in OSTP is that depicted in Figures S8A and

838 S8C. As with the other two cases above, we are equally looking at the OSTP as defined by the

839 continuous input of carbon. Here the rate of input of hydrocarbons into the OSTP per unit time is

840 C_0^{in}. At this influx value per unit time, nitrogen would be the limiting element for microbial

841 growth. In this scenario, we have microbes growing to B_0, a point where they can maximize they

842 nitrogen intake. Carbon in turn changes to a value that is greater than C_2^{in}.

843　　The scenarios in Figures S7C and S7D simulate EPL conditions because $C_T^{in} = 0$. With

844 extended time, C_T will approach a minimum (theoretically zero) as C_T is converted to CH_4 and

845 dead biomass is likewise degraded after labile hydrocarbons are depleted. Figure S7C describes a

846 scenario where the ratio of the nitrogen carrying capacity to carbon carrying capacity of the pond

847 is $< \theta r$. Since there is no supply of exogenous carbon to the system, when the bacteria degrade

848 all residual diluent, they ultimately have no carbon source other than dead biomass, which is

849 converted to CH_4 and CO_2; eventually gas generation ceases in this closed system. Figure S7D

850 predicts the situation where the ratio of the nitrogen carrying capacity to carbon carrying

851 capacity of the pond is $> \theta r$ but C_T still approaches zero because of the complete conversion of

852 C_T and $\beta_T dB$ to gases, where β_T is the proportion of C_T contained in dead biomass that is

853   available for microbial recycling. Note that in the interim, biomass was greater than in Figure

854   S7C because of the continuous presence of N_A.

855 **REFERENCES:**

856 AER, 2018. Statistical series ST 39 monthly report [WWW Document]. URL
857   https://aer.ca/providing-information/data-and-reports/statistical-reports/st39 (accessed
858   4.24.19).

859 Burkus, Z., Wheler, J., Pletcher, S., 2014. GHG emissions from oil sands tailings ponds:
860   Overview and modelling based on fermentable substrates. Alberta Environ. Sustain. Resour.
861   Dev. https://doi.org/10.7939/R3F188

862 Codeco, C.T., Grover, J.P., 2001. Competition along a spatial gradient of resource supply: a
863   microbial experimental model. Am. Nat. 157, 300–315.

864 Connolly, J.P., Coffin, R.B., Landeck, R.E., 1992. Modeling carbon utilization by bacteria in
865   natural water systems. In: Hurst, C. J. (Ed.), Modelling the Metabolic and Physiologic
866   Activities of Microorganisms. John Wiley, New York, 249–276.

867 Del Giorgio, P.A., Cole, J.J., 1998. Bacterial growth efficiency in natural aquatic systems. Annu.
868   Rev. Ecol. Syst. 29, 503–541.

869 Foght, J.M., Gieg, L.M., Siddique, T., 2017. The microbiology of oil sands tailings: Past,
870   present, future. FEMS Microbiol. Ecol. https://doi.org/10.1093/femsec/fix034

871 Roberts, D.J., 2002. Methods for assessing anaerobic biodegradation potential. In: Hurst, C.J.,
872   Crawford, R.L., Knudson, G.R., McInerney, M.J., Stetzenbach, L.D. (Eds.), Manual of
873   Environmental Microbiology, second ed. ASM Press, USA, pp.1008–1017.

874 Mohamad Shahimin, M.F., Foght, J.M., Siddique, T., 2016. Preferential methanogenic
875   biodegradation of short-chain n-alkanes by microbial communities from two different oil
876   sands tailings ponds. Sci. Total Environ. 553, 250–257.

877 Mohamad Shahimin, M.F., Siddique, T., 2017a. Methanogenic biodegradation of paraffinic
878   solvent hydrocarbons in two different oil sands tailings. Sci. Total Environ. 583, 115–122.

879 Mohamad Shahimin, M.F., Siddique, T., 2017b. Sequential biodegradation of complex naphtha
880   hydrocarbons under methanogenic conditions in two different oil sands tailings. Environ.
881   Pollut. 221, 398–406.

882 Siddique, T., Fedorak, P.M., Foght, J.M., 2006. Biodegradation of short-chain n-alkanes in oil
883   sands tailings under methanogenic conditions. Environ. Sci. Technol. 40, 5459–5464.

884 Siddique, T., Fedorak, P.M., MacKinnon, M.D., Foght, J.M., 2007. Metabolism of BTEX and
885   naphtha compounds to methane in oil sands tailings. Environ. Sci. Technol. 41, 2350–2356.

886 Siddique, T., Kuznetsov, P., Kuznetsova, A., Arkell, N., Young, R., Li, C., Guigard, S.,

887   Underwood, E., Foght, J.M., Raymond, J., Grunden, A.M., 2014. Microbially-accelerated
888   consolidation of oil sands tailings. Pathway I: changes in porewater chemistry. Front.
889   Microbiol. 5, 106. https://doi.org/10.3389/fmicb.2014.00106

890   Sterner, R.W., Elser, J.J., 2002. Ecological stoichiometry: the biology of elements from
891   molecules to the biosphere. Princeton University Press.

892   Symons, G.E., Buswell, A.M., 1933. The methane fermentation of carbohydrates1, 2. J. Am.
893   Chem. Soc. 55, 2028–2036.

894   Wang, H., Jiang, L., Weitz, J.S., 2009. Bacterivorous grazers facilitate organic matter
895   decomposition: a stoichiometric modeling approach. FEMS Microbiol. Ecol. 69, 170–179.

896 **Table S1:** Biodegradation and cumulative CH_4 production in cultures of Syncrude MFT
897 incubated with Syncrude naphtha diluent.

Hydrocarbon (mg L^{-1})	Incubation period (days)									
	28	77	142	216	249	271	365	475	605	730
Toluene	46.0	38.2	0	0	0	0	0	0	0	0
Ethylbenzene	19.0	21.6	15.2	0	0	0	0	0	0	0
m-,p-Xylenes	35.0	46.2	35.0	36.9	28.7	10.1	7.7	0	0	0
o-Xylene	14.0	17.7	11.3	0	0	0	0	0	0	0
n-Hexane	5.0	2.5	2.7	1.2	0.7	0.4	0.4	0.3	0.3	0
n-Heptane	34.0	18.2	13.9	6.5	3.7	2.3	1.0	2.6	0	0
n-Octane	46.0	30.2	23.9	13.8	8.0	4.5	2.5	0	0	0
n-nonane	15.0	15.2	6.2	3.5	1.3	0	0	0	0	0
2-Methylhexane (2-MC$_6$)	10.0	6.8	6.0	6.9	6.4	5.3	4.7	5.7	2.7	1.6
3-Methylhexane (3-MC$_6$)	12.0	8.2	7.7	6.7	5.5	2.4	3.2	2.7	1.9	1.9
2-Methylheptane (2MC$_7$)	37.0	25.0	22.1	25.5	23.8	19.7	17.3	21.3	10.2	5.8
4-Methylheptane (4-MC$_7$)	14.0	9.6	8.4	8.4	4.4	3.5	4.4	4.5	3.4	0
Cumulative CH$_4$ production (μmol) *	16	114	416	774	955	893	1049	1039	1266	1248

898 * Cumulative methane is calculated by subtracting CH_4 produced by parallel endogenous control
899 cultures (i.e., MFT not receiving additional naphtha) from CH_4 measured in test cultures (MFT
900 receiving naphtha).

901 **Table S2**: Literature values for selected microbial parameters in system of equations (2)

Parameter *	Value Range	Unit	References
$\boldsymbol{\mu}$	1-4	d^{-1}	(Codeco and Grover, 2001; Connolly et al., 1992)
$\boldsymbol{r}$	0.31-0.75	– §	(Del Giorgio and Cole, 1998; Wang et al., 2009)
$\boldsymbol{\theta}$	$\dfrac{1}{9} - \dfrac{1}{4}$	– §	(Sterner and Elser, 2002)

902 * see Table 1, main text, for parameter definitions
903 –, unitless parameters

904 **Table S3**: Normalized mean square error (NMSE) values obtained by comparing the simulated
905 biodegradation kinetics (generated using the system of equations (2) and parameter values in
906 Table S4) to published experimental data for the 15 labile hydrocarbons (Table 2).
907

Hydrocarbon *	NMSE
n-Pentane	0.92
n-Hexane	0.99
n-Heptane	0.99
n-Octane	0.99
n-Nonane	0.98
n-Decane	0.99
Toluene	1.00
o-Xylene	1.00
m- plus *p*-Xylene	0.99
2-Methylpentane	1.00
3-Methylhexane	0.99
2-Methylheptane	0.95
4-Methylheptane	0.98
2-Methyloctane	0.85

908 *, NMSE values for 2-methylhexane, 2-methyloctane and 2-methylnonane cannot be calculated
909 because the model-related parameter values for these hydrocarbons are not available from our
910 laboratory experiments.

911 **Table S4:** Model parameters and their estimated values obtained from fitting data to the
912 solutions of the systems of equation (3).
913

Parameter *	Value	95% C.I.	Unit
$B(0)$	0.0004	0.0001-0.0138	mmol C
K_f	0.3	0.3	mmol
N_T	327.6	327.1	mmol
$K_{g_{C_5}}$	56.3	16.2-96.4	mmol
$K_{g_{C_6}}$	430.3	366.1-494.5	mmol
$K_{g_{C_7}}$	270.7	238.9-302.5	mmol
$K_{g_{C_8}}$	90.1	69.3-110.9	mmol
$K_{g_{C_9}}$	0.9	0.71-1	mmol
$K_{g_{C_{10}}}$	12.0	10.2-13.9	mmol
$K_{g_{toluene}}$	4.5	4.1-4.8	mmol
$K_{g_{m,p-Xylenes}}$	85.1	76.9-93.2	mmol
$K_{g_{o-Xylenes}}$	17.5	14.2-20.8	mmol
$K_{g_{2-MC_6}}$ §	144.6	102.7-186.5	mmol
$K_{g_{3-MC_6}}$	144.6	102.7-186.5	mmol
$K_{g_{2-MC_7}}$	320.4	183.8-457.1	mmol
$K_{g_{4-MC_7}}$	170.3	121.0-219.7	mmol
$K_{g_{2-MC_8}}$	335.9	179.1-492.9	mmol
$K_{g_{3-MC_8}}$ §	335.9	179.1-492.9	mmol
$K_{g_{2-MC_9}}$ §	335.9	179.1-492.9	mmol
$K_{g_{2-MC_5}}$	165.9	130.2-201.7	mmol
$C_5 - lag$	200	200	days
$C_6 - lag$	26	26	days
$C_7 - lag$	60	40-80	days
$C_8 - lag$	60	60	days
$C_9 - lag$	70	70	days
$C_{10} - lag$	5	5	days
$Toluene - lag$	30	30	days
$m-$ and p $- Xylenes - lag$	70	70	days
$o - Xylenes - lag$	60	60	days
$2 - MC_6 - lag$ §	25	25	days
$3 - MC_6 - lag$	25	25	days
$2 - MC_7 - lag$	25	25	days
$4 - MC_7 - lag$	25	25	days

$2 - MC_8 - lag$	25	25	days
$3 - MC_8 - lag$ §	25	25	days
$2 - MC_9 - lag$ §	25	25	days
$2 - MC_5 - lag$	23	23	days

914

915 * K_f represents the nitrogen-dependent half-saturation constant for microbial growth; N_T is the
916 total nitrogen available in the system; $K_{g_{C_5}}, K_{g_{C_6}}, K_{g_{C_7}}, K_{g_{C_8}}, K_{g_{C_9}}, K_{g_{C_{10}}}, K_{g_{toluene}},$

917 $K_{g_{o-Xylenes}},$

918 $K_{g_{m,p-Xylenes}}, K_{g_{2-MC_6}}, K_{g_{3-MC_6}}, K_{g_{2-MC_7}}, K_{g_{4-MC_7}}, K_{g_{2-MC_8}}, K_{g_{3-MC_8}}, K_{g_{2-MC_8}}, K_{g_{2-MC_9}},$

919 $K_{g_{2-MC_5}}$ respectively represent the half-saturation constants for microbial growth on C_5-, C_6-,
920 C_7-, C_8-, C_9-, C_{10}- n-alkanes, toluene, o-xylene, m- plus p-xylene, 2-methylhexane-, 3-
921 methylhexane-, 2-methylheptane-, 4-methylheptane-, 2-methyloctane-, 3-methyloctane-, 2-
922 methylnonane- and , 2-methylpentane-. Z-lag denotes a lag period of Z, where Z is one of C_5, C_6,
923 C_7, C_8, C_9, C_{10}, toluene, o-xylene, m- plus p-xylene, 2-methylhexane-, 3-methylhexane, 2-
924 methylheptane, 4-methylheptane, 2-methyloctane 3-methyloctane, 2-methylnonane or 2-
925 methylpentane.

926

927 § The values of model parameters K_g and lag for 2-MC$_6$, 3-MC$_8$ and 2-MC$_9$ were not available
928 from empirical studies and are assumed to be the same as those for 3-MC$_6$, 2-MC$_8$ and 2-MC$_8$,
929 respectively, based on their similar molecular weights.

930 **Table S5**: Estimated zero-and first-order model parameter values for labile diluent hydrocarbons
931 not reported by Siddique et al. (2008).
932

Hydrocarbon	Lag phase (d)	Zero-order parameter (mmole d^{-1})	First-order parameter (d^{-1})
n-Pentane	294	0.0008576	0.01117
n-Nonane	77	2.664e-05	0.01276
2-Methylpentane	600	0.0002281	0.003501
3-Methylhexane	455	0.0001816	0.003849
2-Methylheptane	845	0.00023	0.005258
4-Methylheptane	665	0.0001936	0.005663
2-Methyloctane	665	0.0001772	0.0006584

933

934 **Table S6.** Calculation of mass balance of diluent entering OSTP in 2016 and 2017. These values
935 are used in Table S8 calculations.

936

	Syncrude MLSB		CNRL Horizon		CNUL MRM	
	2016	2017	2016	2017	2016	2017
Reported mass of diluent lost to fresh tailings before deposition in OSTP (t) [a]	57,336	43,032	24,722	35,295	28,558	32,494
Estimated mass of diluent lost from OSTP by volatilization (t) [b]	(-17,201)	(-12,910)	(-7,416)	(-10,589)	(-11,423)	(-12,998)
Calculated net mass of diluent remaining in OSTP (t)	40,135	30,122	17,305	24,706	17,135	19,496

937
938 a, Data retrieved from Alberta Energy Regulator ST 39 report (AER, 2018) and calculated using
939 the reported volume of diluent loss (m^3) and multiplying by the respective densities of diluents
940 (Syncrude naphtha, 0.76 t m^{-3}; CNRL naphtha, 0.73 t m^{-3}; and CNUL paraffinic solvent, 0.65 t
941 m^{-3} (Burkus et al., 2014).
942 b, A factor of 0.7 (i.e., 30% volatilization) was used for Syncrude and CNRL naphtha diluents
943 and a factor of 0.6 (i.e., 40% volatilization) was used for CNUL paraffinic diluent to calculate
944 the mass of diluent volatilized from OSTP per Burkus et al. (2014) .

Table S7. Concentrations of 18 labile hydrocarbons in diluents and calculated masses of labile diluent hydrocarbons present in tailings entering OSTP in 2016 and 2017. Values are used in Table S8 calculations.

Labile hydrocarbon	Syncrude MSLB			CNRL Horizon			CNUL MRM		
	% of naphtha diluent [a]	mass in OSTP (t) 2016 [b]	mass in OSTP (t) 2017 [b]	% of naphtha diluent [a]	mass in OSTP (t) 2016 [b]	mass in OSTP (t) 2017 [b]	% of paraffinic diluent [a]	mass in OSTP (t) 2016 [b]	mass in OSTP (t) 2017 [b]
Toluene	6.11	2452	1840	0	0	0	0	0	0
m-, *p-*Xylene	4.64	1862	1398	0	0	0	0	0	0
*o-*Xylene	1.78	714	536	0	0	0	0	0	0
n-C$_5$	0	0	0	0	0	0	24.00	4112	4679
n-C$_6$	0.60	241	181	3.85	666	951	11.26	1929	2195
n-C$_7$	4.50	1806	1356	9.35	1618	2310	0	0	0
n-C$_8$	6.05	2428	1822	4.65	805	1149	0	0	0
n-C$_9$	1.99	799	599	1.70	294	420	0	0	0
n-C$_{10}$	0.31	126	94	1.65	286	408	0	0	0
2-MC$_5$	0	0	0	1.25	216	309	23.50	4027	4582
2-MC$_6$	1.30	522	392	5.30	917	1309	0	0	0
3-MC$_6$	1.51	607	456	5.05	874	1248	0	0	0
2-MC$_7$	4.92	1976	1483	3.85	666	951	0	0	0
4-MC$_7$	1.86	747	561	1.25	216	309	0	0	0
2-MC$_8$	1.16	465	349	1.00	173	247	0	0	0
3-MC$_8$	1.55	623	467	0.55	95	136	0	0	0
2-MC$_9$	0.31	124	93	2.90	502	717	0	0	0
% of diluent considered labile	39			42			59		
Total mass of labile hydrocarbon entering OSTP (t)		15492	11627		7329	10463		10068	11456

[a] The concentrations of individual hydrocarbons in Syncrude and CNRL naphtha diluents were calculated using PONAU analysis reported by (Siddique et al., 2007) and (Mohamad Shahimin, and Siddique, 2017b), respectively, and the concentrations of individual hydrocarbons in CNUL paraffinic diluent were calculated using the PONAU analysis reported by (Mohamad Shahimin and Siddique, 2017a).

[b] The data were retrieved from Alberta Energy Regulator report ST 39 (AER, 2018)

956 **Table S8:** Contribution of individual labile diluent hydrocarbons to the maximum theoretical
957 cumulative yield of CH_4 from OSTPs in 2016 and 2017, based on masses calculated in Tables S5
958 and S6). Methane yield was calculated using equation (4) in main text, per Symons and Buswell
959 (1933) as implemented by Roberts (2002).

Labile hydrocarbon	Calculated theoretical methane production (moles x 10^6)					
	Syncrude MLSB	CNRL Horizon	CNUL MRM	Syncrude MLSB	CNRL Horizon	CNUL MRM
	2016			**2017**		
Toluene	120	0	0	90	0	0
m-, *p*-Xylene	92	0	0	69	0	0
o-Xylene	35	0	0	27	0	0
n-C$_5$	0	0	228		0	259
n-C$_6$	13	37	106	10	52	121
n-C$_7$	99	89	0	74	127	0
n-C$_8$	133	44	0	100	63	0
n-C$_9$	44	16	0	33	23	0
n-C$_{10}$	7	16	0	5	22	0
2-MC$_5$	0	12	222	0	17	253
2-MC$_6$	29	50	0	21	72	0
3-MC$_6$	33	48	0	25	69	0
2-MC$_7$	108	36	0	81	52	0
4-MC$_7$	41	12	0	31	17	0
2-MC$_8$	25	9	0	19	14	0
3-MC$_8$	34	5	0	25	7	0
2-MC$_9$	7	27	0	5	39	0
Total theoretical methane (moles x 10^6) [a]	820	401	556	615	574	633
Microbial hydrocarbon conversion to methane (moles x 10^6) [b]	656	321	445	492	459	506
Total methane emissions from ponds (moles x 10^6) [c]	1191	336	2634	991	599	1051
Contribution of diluent hydrocarbons to total methane emissions from ponds (%)	55	95	17	50	77	48

960 [a] The masses of individual hydrocarbons from Table S6 were converted into moles using the respective molecular
961 weights and then Symons and Buswell equation (per Roberts, 2002) was used to calculate theoretical maximum
962 methane production from individual hydrocarbons.
963 [b] A factor of 0.8 determined during our hydrocarbon biodegradation studies (Siddique et al., 2007, 2006) was used
964 to calculate the efficiency of microbial conversion of hydrocarbons to methane; i.e., r_i
965 [c] CH_4 emission data (unpublished data, Government of Alberta) were converted into moles for comparison. The
966 Government of Alberta data includes CH_4 emissions from all units. We considered only those units that had been
967 receiving froth treatment tailings (solvent containing stream) for the most recent two or three years. Therefore, for
968 comparison, the bubbling zone of Syncrude MLSB, the entire CNRL Horizon pond and Cells 1-3 of CNUL
969 receiving diluent containing streams were used for field emissions data.
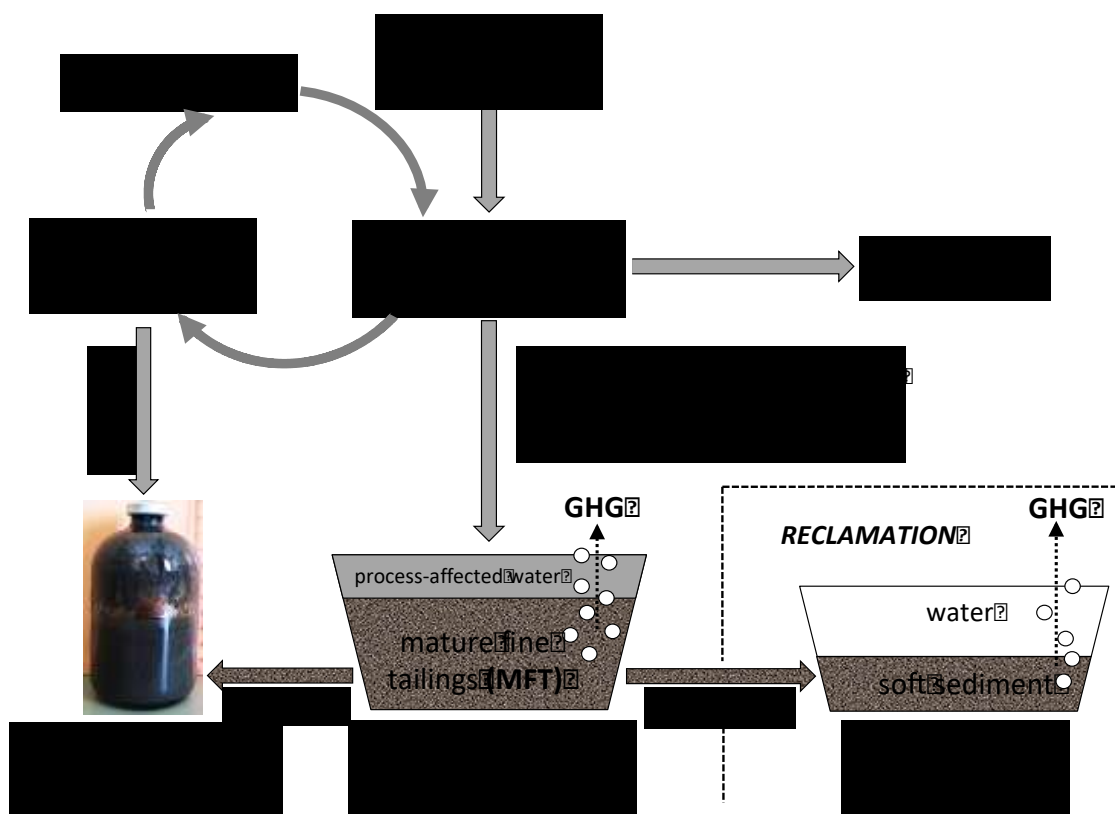
Figure S1. Simplified schematic of aqueous bitumen extraction from surface-mined oil sands, with subsequent retention of tailings in oil sands tailings ponds (OSTP) and reclamation in end pit lakes (EPL) (reviewed Foght et al., 2017). Biogenic gases in tailings (1) may escape to the atmosphere from shallow sediments via ebullition as greenhouse gas (GHG) emissions during retention or from deeper sediments when physically disturbed (e.g., by mechanical transfer), or (2) may be trapped as temporary or permanent gas voids (Guo, 2009) in dense sediments as latent GHG emissions, or (3) may be immobilized and transformed via geochemical interactions with clay minerals and pore water (Siddique et al., 2014).

980
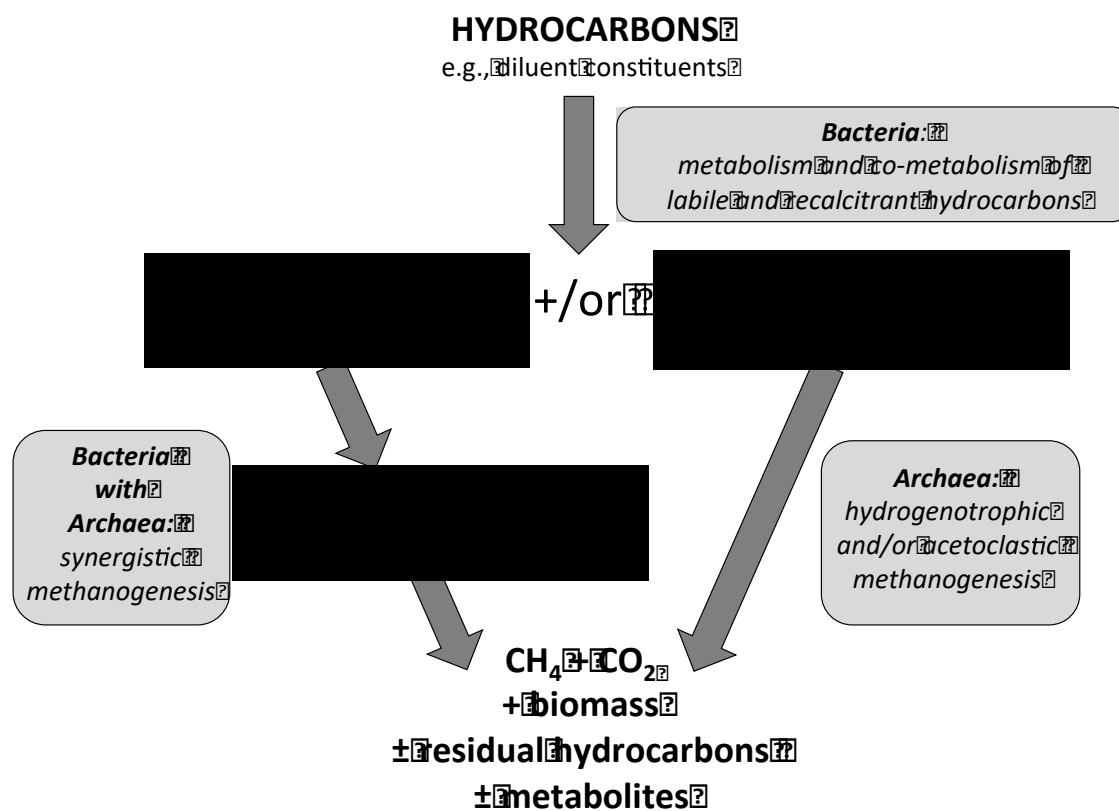
981
982 **Figure S2.** Simplified biochemical flowchart for methanogenic biodegradation of hydrocarbons.
983 Metabolic processes carried out by bacteria or archaea alone or by synergistic consortia are
984 indicated in italics. If sulfate is present in sufficient concentrations (e.g., via addition of gypsum
985 [$CaSO_4 \cdot 2H_2O$] in some oil sands tailing processes; Foght et al., 2017), anaerobic biodegradation
986 may still proceed but will be skewed toward accumulation of metabolites plus CO_2 and biomass,
987 with minimal CH_4 production. The ultimate end products include GHG, biomass, non-degradable
988 hydrocarbons and dead-end metabolites, e.g., from partial oxidation of recalcitrant hydrocarbons.
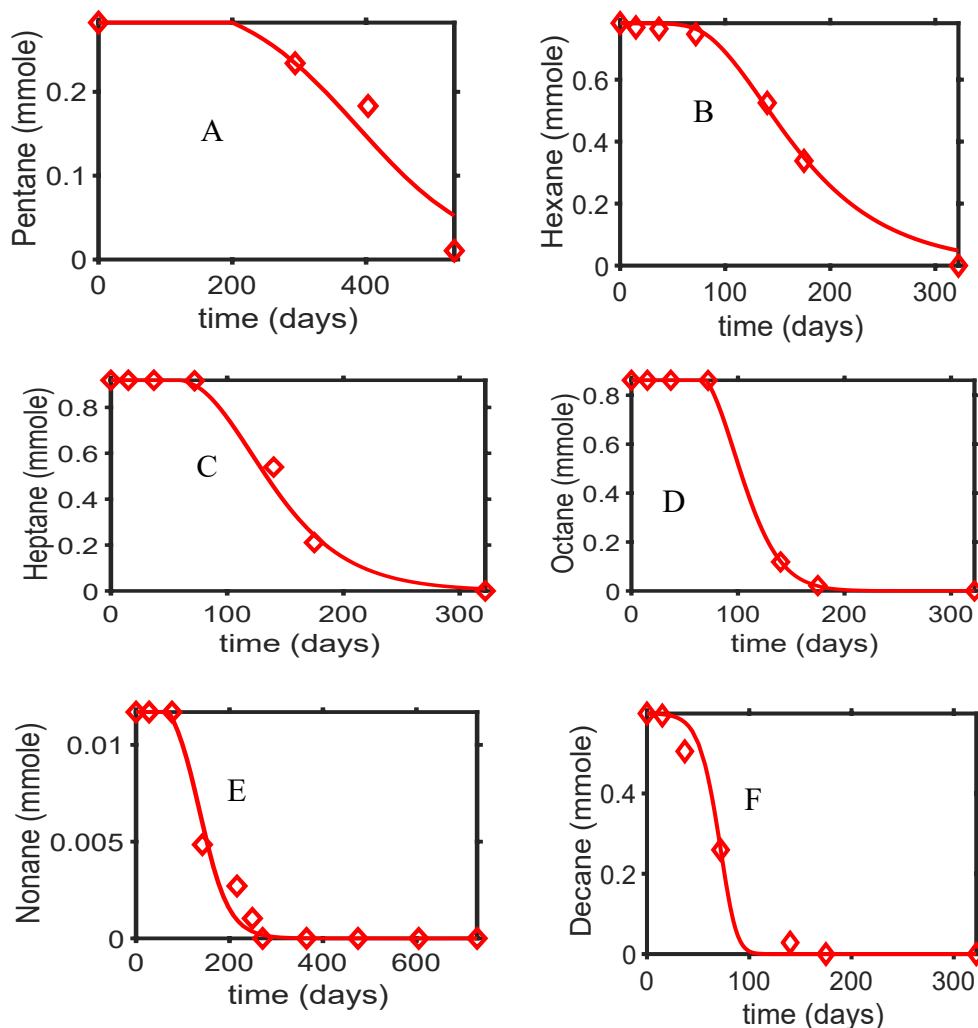
989

990 **Figure S3.** System of equations (2) fit to measured *n*-alkane biodegradation values for laboratory
991 cultures. Symbols denote measured values and lines represent best fits to the data. Panels A, B,
992 C, D, E and F show results for *n*-pentane, *n*-hexane, *n*-heptane, *n*-octane, *n*-nonane, and *n*-
993 decane, respectively.
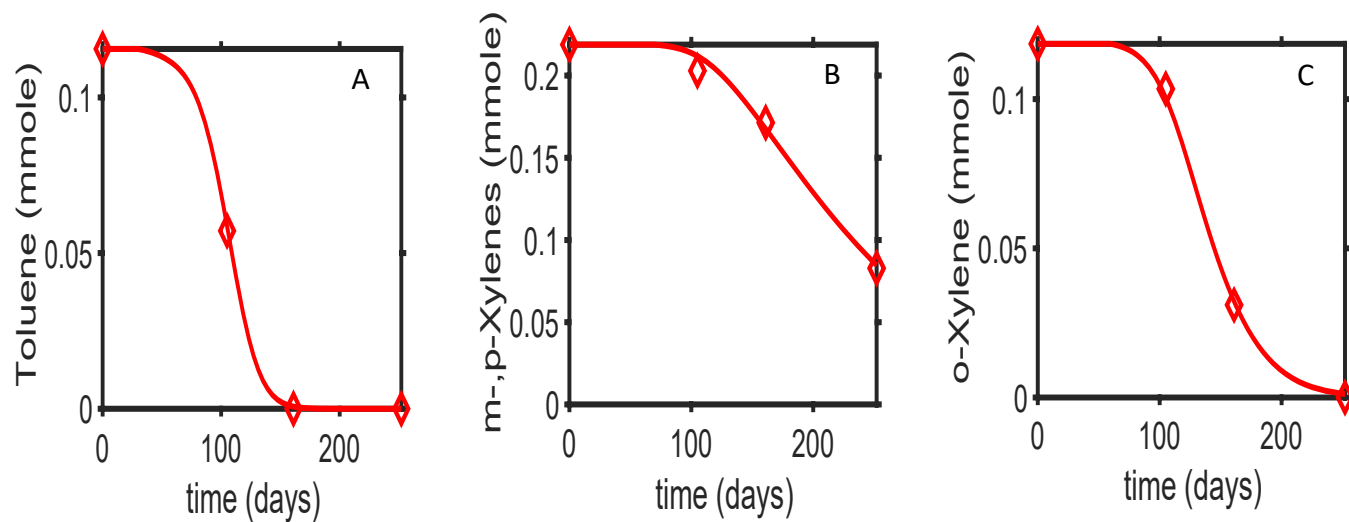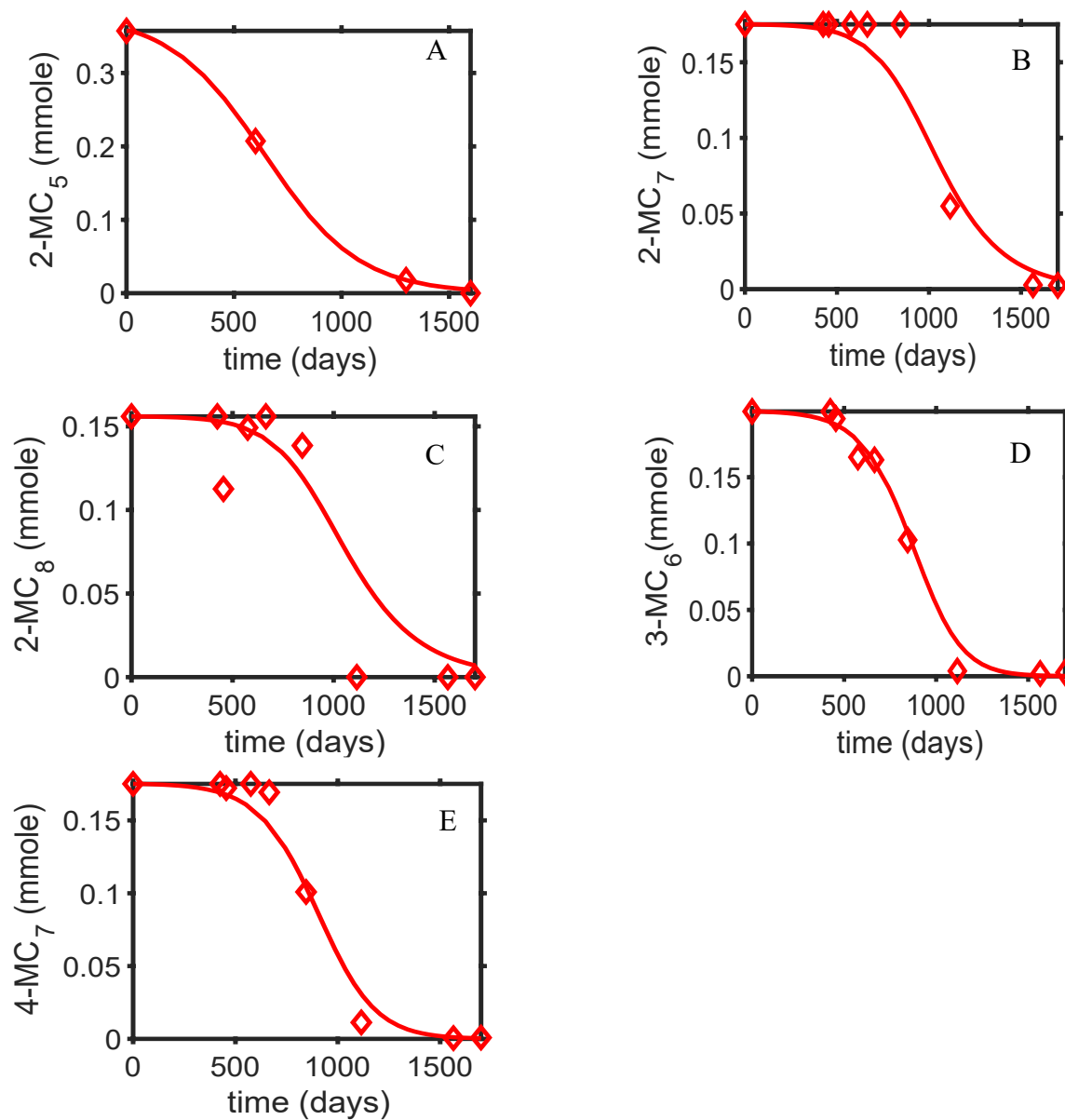
994

995

996

997

998

999

1000

1001

1002

1003

Figure S4. System (2) fit to measured biodegradable monoaromatic compound data for laboratory cultures. Diamond symbols denote measured values and solid lines represent fitted values. Panels A, B and C respectively show results for toluene, *m*- plus *p*-xylene, and *o*-xylene.

1007

1008
1009
1010
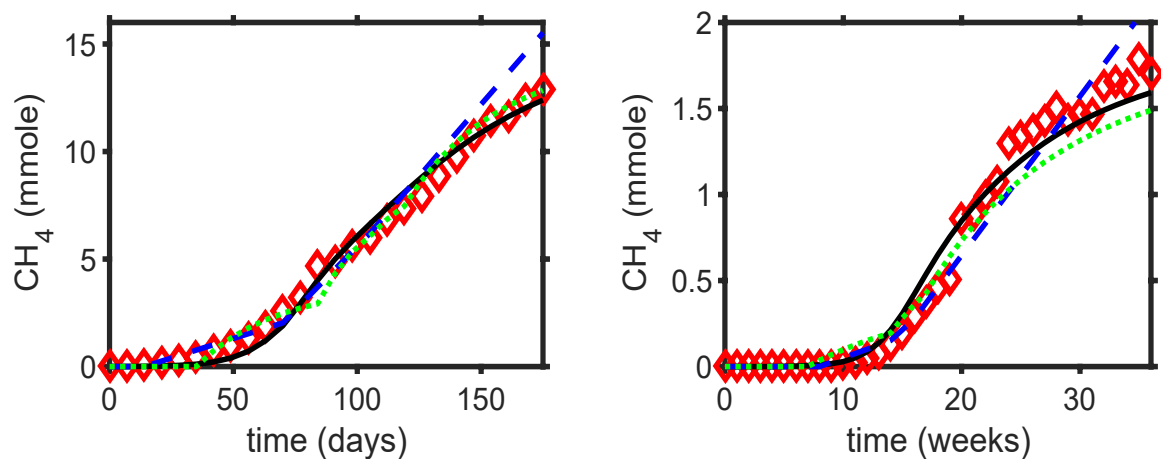1011
1012 **Figure S5.** System (2) fit to *iso*-alkane biodegradation measurements for laboratory cultures.
1013 Solid lines represent fitted values and diamonds denote measured values. Panels A, B, C, D and
1014 E show results for 2-methylheptane, 2-methyloctane, 2-methylpentane, 3-methylhexane and 4-
1015 methylheptane, respectively.

Figure S6: Comparison of stoichiometric model predictions of methane production from laboratory cultures of Syncrude MFT incubated with mixtures of either n-alkane (C_6, C_7, C_8 and C_{10}) or monoaromatic (toluene, o-, m- and p-xylenes) components of naphtha diluent (left and right panels, respectively). Measured methane values, from laboratory experiments independent of those used to develop the model, are shown by diamond symbols. Solid black lines represent the stoichiometric model prediction; broken blue lines and dotted green lines respectively represent predictions made by using the previous zero-order and first-order models (Siddique et al., 2008).
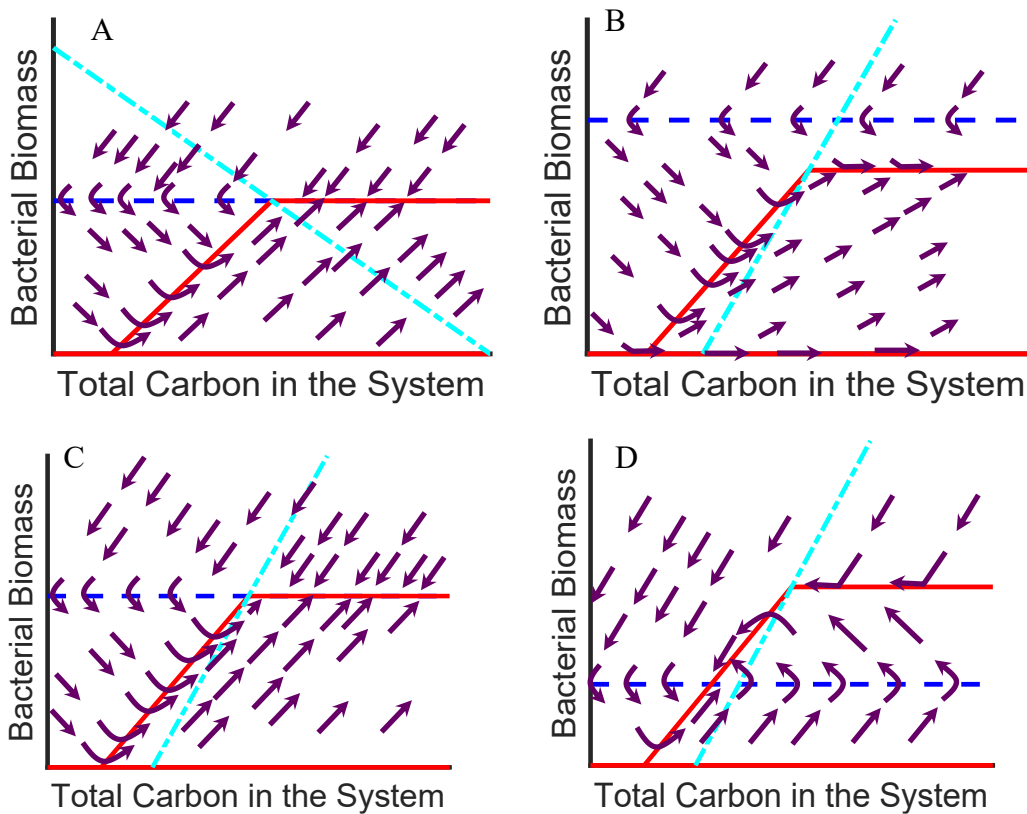
1026
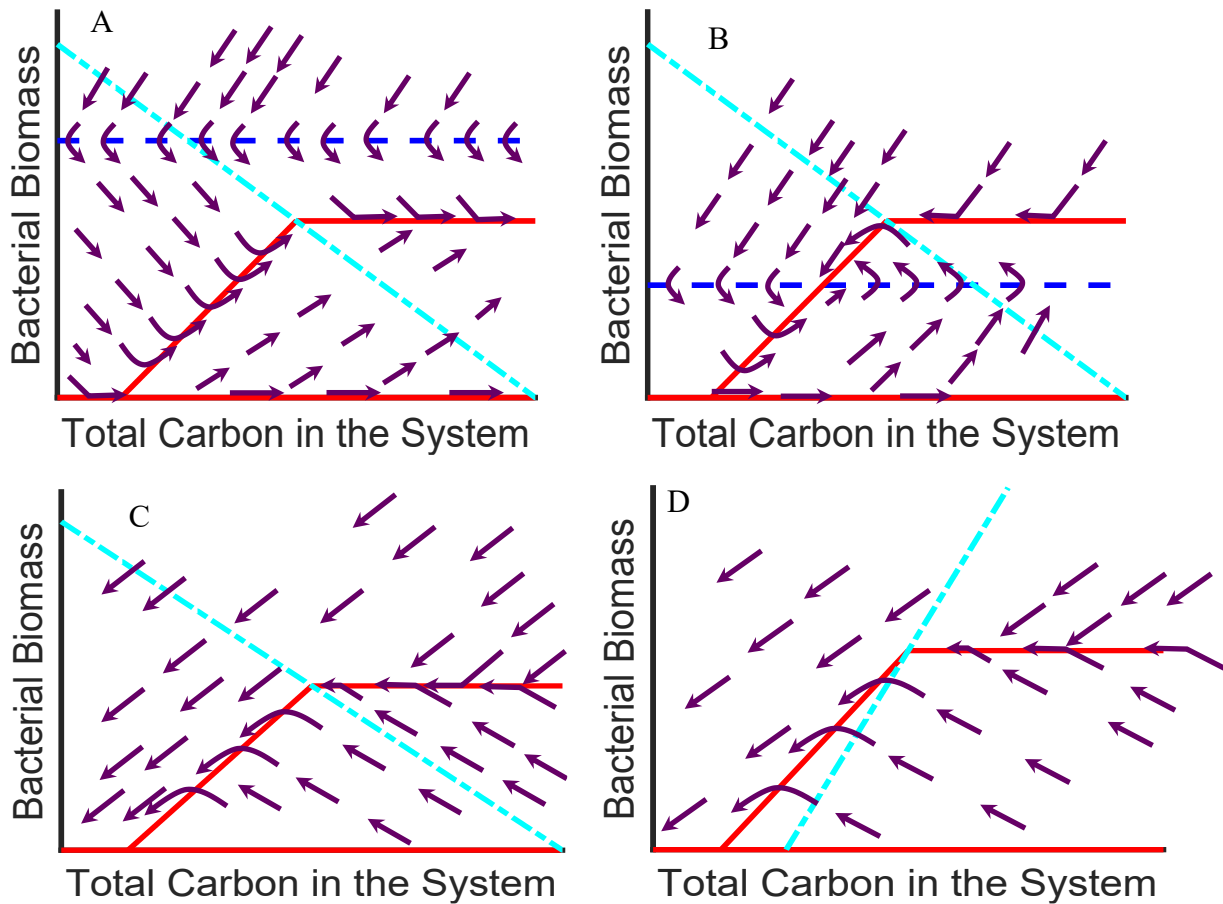
1027

1028

1029 **Figure S7:** Phase plane analysis of solution states for microbial biomass and total carbon content
1030 in OSTP (Panels A and B, where $C^{in} > 0$) or EPL (Panels C and D, where $C_T^{in} = 0$) under
1031 different assumed initial conditions of $C_T{}^{in}$ and ratio of the nitrogen carrying capacity to carbon
1032 carrying capacity $(k_f : k_g)$. In Panel A: $C_T^{in} > \left(N_T - \frac{dk_f}{\mu}\right)\frac{d(1-r)}{\theta r}$ and $k_f : k_g < \theta r$. In Panel B,
1033 $C_T^{in} < \left(N_T - \frac{dk_f}{\mu}\right)\frac{d(1-r)}{\theta r}$ and $k_f : k_g < \theta r$. In Panel C: $k_f : k_g < \theta r$. In Panel D: $k_f : k_g > \theta r$.
1034 Solid red lines are nullclines for total biomass, broken blue lines are nullclines for total carbon
1035 content and broken light blue lines indicate where $B = \left(N_T - \frac{\left(C_T + \frac{B}{r}\right)k_f}{k_g}\right)\left(\frac{k_g r}{\theta k_g r - k_f}\right)$, to the left of
1036 which nitrogen is limiting and to the right of which carbon is limiting. The slope of this line is
1037 determined by the ratio: $k_f : k_g$. Purple directional arrows account for time.

1038

1039

1040

1041

1042 **Figure S8:** Phase plane analysis of solution states for microbial biomass and total carbon content
1043 in OSTP (where $C^{in} > 0$) under different assumed initial conditions of C_T^{in} and ratio of the
1044 nitrogen carrying capacity to carbon carrying capacity ($k_f : k_g$). In Panel A: $C_T^{in} =$
1045 $\left(N_T - \frac{dk_f}{\mu}\right)\frac{d(1-r)}{\theta r}$ and $k_f : k_g < \theta r$. In Panel B, $C_T^{in} > \left(N_T - \frac{dk_f}{\mu}\right)\frac{d(1-r)}{\theta r}$ and $k_f : k_g > \theta r$. In
1046 Panel C: $C_T^{in} = \left(N_T - \frac{dk_f}{\mu}\right)\frac{d(1-r)}{\theta r}$ and $k_f : k_g > \theta r$. In Panel D: $C_T^{in} < \left(N_T - \right.$
1047 $\left. \frac{dk_f}{\mu}\right)\frac{d(1-r)}{\theta r}$ and $k_f : k_g > \theta r$. Solid red lines are nullclines for total biomass, broken blue lines
1048 are nullclines for total carbon content and broken light blue lines indicate where the line $B =$
1049 $\left(N_T - \frac{\left(C_T + \frac{B}{r}\right)k_f}{k_g}\right)\left(\frac{k_g r}{\theta k_g r - k_f}\right)$ to the left of which nitrogen is limiting and to the right of which
1050 carbon is limiting. The slope of this line is determined by the ratio: $k_f : k_g$. Purple directional
1051 arrows account for time.